LETTER

Dopamine enhances signal–to–noise ratio in cortical–brainstem encoding of aversive stimuli

Caitlin M. Vander Weele[1,4], Cody A. Siciliano[1,4], Gillian A. Matthews[1,4], Praneeth Namburi[1], Ehsan M. Izadmehr[1], Isabella C. Espinel[1], Edward H. Nieh[1], Evelien H. S. Schut[1,2], Nancy Padilla-Coreano[1], Anthony Burgos-Robles[1], Chia-Jung Chang[1], Eyal Y. Kimchi[1], Anna Beyeler[1], Romy Wichmann[1,3], Craig P. Wildes[1] & Kay M. Tye[1,3]*

Dopamine modulates medial prefrontal cortex (mPFC) activity to mediate diverse behavioural functions[1,2]; however, the precise circuit computations remain unknown. One potentially unifying model by which dopamine may underlie a diversity of functions is by modulating the signal-to-noise ratio in subpopulations of mPFC neurons[3–6], where neural activity conveying sensory information (signal) is amplified relative to spontaneous firing (noise). Here we demonstrate that dopamine increases the signal-to-noise ratio of responses to aversive stimuli in mPFC neurons projecting to the dorsal periaqueductal grey (dPAG). Using an electrochemical approach, we reveal the precise time course of pinch-evoked dopamine release in the mPFC, and show that mPFC dopamine biases behavioural responses to aversive stimuli. Activation of mPFC–dPAG neurons is sufficient to drive place avoidance and defensive behaviours. mPFC–dPAG neurons display robust shock-induced excitations, as visualized by single-cell, projection-defined microendoscopic calcium imaging. Finally, photostimulation of dopamine terminals in the mPFC reveals an increase in the signal-to-noise ratio in mPFC–dPAG responses to aversive stimuli. Together, these data highlight how dopamine in the mPFC can selectively route sensory information to specific downstream circuits, representing a potential circuit mechanism for valence processing.

Despite the popularity of the signal-to-noise ratio (SNR) model for mPFC dopamine in computational and theoretical neuroscience, the degree to which it translates across brain functions is unknown. Evidence supporting dopamine-mediated SNR modulations have been found in ex vivo preparations[4], and in vivo during auditory stimulus discrimination[7], visual stimulus discrimination[8] and working memory[9]. As mPFC neurons respond to both rewarding and aversive stimuli[10,11], and dopamine neurons in the ventral tegmental area (VTA) that project to the mPFC (VTA[DA]–mPFC neurons) are uniquely sensitive to aversive stimuli[12–16], we proposed that mPFC neurons encoding aversive or rewarding events are differentially modulated by dopamine.

Dopamine release in the mPFC in response to aversive stimuli has previously been observed with direct but slow[14,17], or fast but indirect[12,16] methodologies. Fast-scan cyclic voltammetry (FSCV) offers a direct measurement of catecholamine neurotransmission with precise temporal resolution, but is rarely used outside the striatum owing to difficulty in discriminating between noradrenaline and dopamine[18]. Here we investigated the precise time course of dopamine release using FSCV combined with optical and pharmacological approaches to dissect contributions of VTA[DA] neurons. Electrodes were aimed at deep layers (5–6) of the mPFC, where VTA[DA] terminals were densest, relative to locus coeruleus (LC) noradrenaline terminals (LC[NA]) (Fig. 1a, b), and secured in locations detecting stimulated dopamine release (Extended Data Fig. 1). In tyrosine hydroxylase (TH)::Cre rats, which expressed halorhodopsin (NpHR) in a Cre-dependent manner in VTA[DA] neurons, we performed tail pinches with and without photoinhibition of VTA[DA] neurons (Fig. 1c). Photoinhibition of VTA[DA]

neurons attenuated the pinch-induced signals in the mPFC (Fig. 1d, e). Further, in a separate group of rats, pharmacological inactivation of the LC did not affect pinch-evoked catecholamine release in the mPFC (Extended Data Fig. 1). These data suggest that VTA[DA]–mPFC neurons contributed the bulk of the rapid pinch-evoked catecholaminergic signal.

Next, we explored the causal relationship between VTA[DA]–mPFC and valence processing by testing whether this circuit component was sufficient to promote aversion. We used TH::Cre rats to express channelrhodopsin-2 (ChR2) in VTA[DA] neurons, and implanted optical fibres over the mPFC (Fig. 1f). Activation of VTA[DA]–mPFC terminals had no effect on behaviour in real-time place avoidance (RTPA) or conditioned place aversion (CPA) assays (Extended Data Fig. 2). However, in light of the model for dopamine involvement in enhancing the SNR, we considered whether dopamine might enhance responses to discrete, predictive cues. We trained rats to associate auditory or visual cues (counterbalanced) with either shock or sucrose delivery. Once rats learned to discriminate the cues predicting shock or sucrose by freezing or approaching the sucrose port, respectively (Extended Data Fig. 2), we tested their behavioural responses to the 'competition' of simultaneously presented cues (Fig. 1g) driving conflicting motivational outputs[10] (Fig. 1h). Photostimulation of VTA[DA]–mPFC (using empirically determined optical parameters, Fig. 1i) during the competition trials caused rats expressing ChR2 to spend significantly less time in the sucrose delivery port and more time freezing compared to controls expressing eYFP (Fig. 1j, k). Taken together, these data suggest that dopamine is released in a time-locked manner upon presentation of an aversive stimulus, and that VTA[DA] in the mPFC biases behavioural responses towards aversion in the face of conflicting motivational drives.

We next sought to identify distinct, anatomically defined subpopulations in the mPFC that might relay information relevant to processing of aversive information. The mPFC has many downstream projection targets, including the periaqueductal grey (PAG) and nucleus accumbens (NAc) (Extended Data Fig. 3). In animal studies, stimulation of the PAG evokes aversive responses, including defensive and attack behaviours[19–21]. While projections to the dorsal PAG (dPAG) have been explored in the context of social behaviour[22], contributions of the mPFC–dPAG circuit to discrete stimulus processing have not yet been evaluated. Owing to its reported role in reward-related processes, we also investigated the mPFC–NAc projection for comparison[23–25]. Consistent with previous results[22], we found that the mPFC–dPAG circuit and mPFC–NAc projections formed anatomically distinct subpopulations (Extended Data Fig. 3).

To target these pathways, ChR2 or eYFP alone was expressed in either mPFC–dPAG or mPFC–NAc neurons (Fig. 2a and Extended Data Fig. 4). Photostimulation of mPFC–NAc neurons did not produce detectable differences in behaviour between ChR2 and eYFP-expressing groups during RTPA or CPA (Extended Data Fig. 4). By contrast,

[1]The Picower Institute for Learning and Memory, Department of Brain and Cognitive Sciences, Massachusetts Institute of Technology, Cambridge, MA, USA. [2]Department of Cognitive Neuroscience, Radboudumc Nijmegen, Nijmegen, The Netherlands. [3]Present address: Salk Institute for Biological Sciences, La Jolla, CA, USA. [4]These authors contributed equally: Caitlin M. Vander Weele, Cody A. Siciliano, Gillian A. Matthews. *e-mail: tye@salk.edu
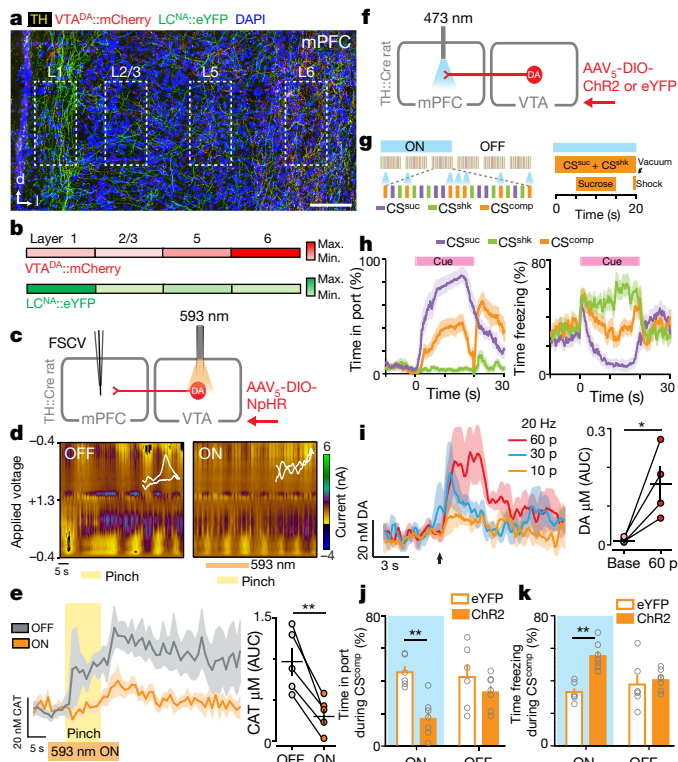
Fig. 1 | Tail pinch evokes rapid dopamine release in the mPFC and dopamine biases behaviour towards aversion during stimulus competition. a, Targeted expression of mCherry in VTA^{DA} neurons (VTA^{DA}::mCherry) and eYFP in LC^{NA} terminals (LC^{NA}::eYFP) in the mPFC. Scale bar, 100 μm. **b**, VTA^{DA} terminals were densest in deep layers. LC^{NA} terminals were densest in superficial layers ($n = 3$ mice). **c**, Strategy to verify dependence of tail-pinch-evoked catecholamine neurotransmission (CAT) on VTA^{DA} neurons. **d**, Representative pseudocolour plots showing tail-pinch-evoked CAT before and during VTA^{DA} inhibition (593-nm laser light, 20 s) ($n = 5$ rats). **e**, Photoinhibition of VTA^{DA} neurons attenuated tail-pinch-evoked CAT release, evident in the average traces (left) and CAT concentration (right). Two-tailed paired t-test, $t_4 = 5.884$, **$P = 0.004$. **f**, Strategy for manipulating dopamine release in the mPFC. **g**, Schematic of competition task. During competition sessions, in addition to sucrose (CS^{suc}, purple) and shock (CS^{shk}, green) trials, sucrose and shock were co-presented as competition trials (CS^{comp}, orange). During ON sessions, VTA^{DA}–mPFC was activated (473 nm, 20 Hz, 60 pulses, every 5 s) during the CS^{comp} trials. During OFF sessions, light was not delivered. **h**, Percentage of time spent in the reward port and freezing during each trial type ($n = 13$ rats). **i**, Evoked dopamine release in the mPFC following 20-Hz optical activation of VTA^{DA} neurons expressing ChR2–mCherry (VTA^{DA}::ChR2–mCherry) ($n = 4$ rats; 60 pulses: two-tailed paired t-test, $t_3 = 3.72$, *$P = 0.034$). Arrow indicates stimulation onset. **j**, Average time spent in the reward port during competition ON trials was lower in VTA^{DA}::ChR2 rats ($n = 7$ rats; closed bars) compared with VTA^{DA}::eYFP control rats ($n = 6$ rats; open bars). Repeated measures, two-way ANOVA, $F_{1,11} = 8.13$, $P = 0.0157$; Bonferroni multiple comparisons tests, **$P = 0.0025$. **k**, Mean time spent freezing during competition ON trials was greater in rats expressing ChR2 compared with rats expressing eYFP. Repeated measures, two-way ANOVA, $F_{1,11} = 13.29$, $P = 0.0039$; Bonferroni multiple comparisons tests, **$P = 0.0013$. Error bars (**e**, **i**–**k**) and shading (**e**, **h**, **i**) represent s.e.m.

activation of ChR2 in mPFC–dPAG neurons reduced the time spent in the light-paired chamber in both RTPA (Fig. 2b) and CPA (Fig. 2c), relative to eYFP controls. In the open-field test, which assays locomotor activity and anxiety-related behaviour, photostimulation of mPFC–dPAG did not affect distance travelled (Fig. 2d) or time spent in the centre of the chamber between ChR2- and eYFP-expressing rats (Extended Data Fig. 5). Strikingly, photostimulation of mPFC–dPAG produced an increase in marble burying and time spent digging (Fig. 2e–h and Supplementary Video 1). The effects in the RTPA and marble-burying assays observed
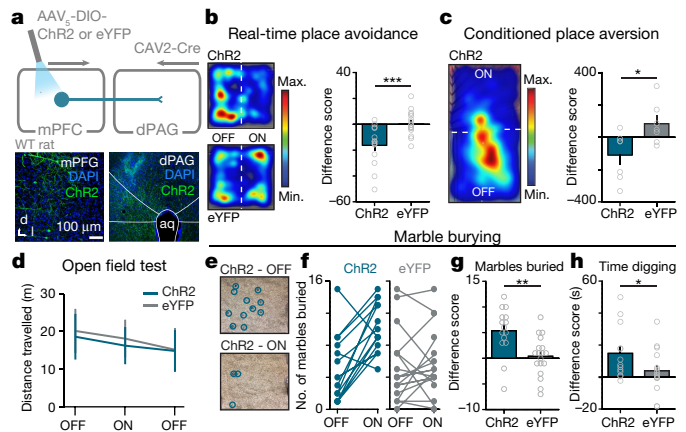

Fig. 2 | The mPFC promotes aversion through projections to the dPAG. a, Top, strategy for optogenetic activation of mPFC neurons projecting to the dPAG in wild-type (WT) rats. Bottom, representative images of the mPFC and dPAG. **b**, Left, representative locomotor heat maps of RTPA in rats expressing ChR2 or eYFP in mPFC–dPAG neurons (mPFC–dPAG::ChR2 or mPFC–dPAG::eYFP rats, respectively). Activation of mPFC–dPAG neurons in mPFC–dPAG::ChR2 rats resulted in increased RTPA ($n = 15$ rats) compared to mPFC–dPAG::eYFP controls ($n = 17$ rats) (right). Difference score = (time spent in the ON zone) – (time spent in the OFF zone). Two-tailed unpaired t-test, $t_{30} = 3.902$, ***$P = 0.0005$. **c**, Left, representative locomotor heat map of a mPFC–dPAG::ChR2 rat on a CPA test day. Right, activation of mPFC–dPAG neurons resulted in increased CPA in mPFC–dPAG::ChR2 rats ($n = 7$ rats) compared to mPFC–dPAG::eYFP controls ($n = 7$ rats). Two-tailed unpaired t-test, $t_{12} = 2.638$, *$P = 0.0217$. **d**, Optogenetic activation of mPFC–dPAG did not change locomotor activity. mPFC–dPAG::ChR2, $n = 15$ rats; mPFC–dPAG::eYFP, $n = 18$ rats. Distance travelled, two-way repeated measures ANOVA, group × epoch interaction, $F_{2,62} = 0.94$, $P = 0.3957$. **e**, Representative arena of mPFC–dPAG::ChR2 rat after marble-burying assay when laser stimulation was OFF or ON. **f**, Number of marbles buried in ON and OFF conditions for mPFC–dPAG::ChR2 or mPFC–dPAG::eYFP rats. **g**, Optogenetic stimulation of mPFC–dPAG neurons resulted in a larger change in the number of marbles buried by mPFC–dPAG::ChR2 rats ($n = 15$ rats) compared to mPFC–dPAG::eYFP controls ($n = 18$ rats). Difference score = (number of marbles buried during ON session) – (number of marbles buried during OFF session). Two-tailed unpaired t-test, $t_{31} = 3.341$, **$P = 0.0022$. **h**, mPFC–dPAG::ChR2 rats ($n = 13$ rats) spent more time digging during optical stimulation in comparison to mPFC–dPAG::eYFP controls ($n = 16$ rats). One-tailed unpaired t-test, $t_{27} = 1.961$, *$P = 0.0301$. Data are mean ± s.e.m.

upon activation of mPFC–dPAG somata were reproduced by activation of mPFC terminals directly in the dPAG (Extended Data Fig. 5).

These data show that optogenetic activation of the mPFC–dPAG projection drives place avoidance and defensive behaviours; however, optogenetic activation may not reflect endogenous circuit function. To address this, we investigated the dynamics of individual neurons in the mPFC–dPAG and mPFC–NAc populations during shock or sucrose presentation. We performed in vivo microendoscopic imaging[26] of neurons expressing a genetically encoded calcium indicator (GCaMP6m)[27]. To visualize changes in intracellular calcium concentration indicative of neural activity, we selectively expressed GCaMP6m in mPFC–dPAG and mPFC–NAc neurons (Fig. 3a). Assessment of bulk fluorescence activity, a measure of population activity, revealed that the mPFC–NAc population was not significantly modulated by either shock or sucrose (Fig. 3b). By contrast, mPFC–dPAG neurons showed a robust, time-locked increase in activity in response to shock and a decrease in response to sucrose (Fig. 3c). To assess the activity of individual projection-defined neurons, we used a constrained non-negative matrix factorization algorithm optimized for microendoscopic imaging (CNMF-E)[28] (Fig. 3d and Supplementary Videos 2, 3). We identified 169 mPFC–NAc and 118 mPFC–dPAG neurons, which sorted into 6 functional clusters (Fig. 3e and Extended Data Fig. 6). When comparing the normalized responses of individual cells within
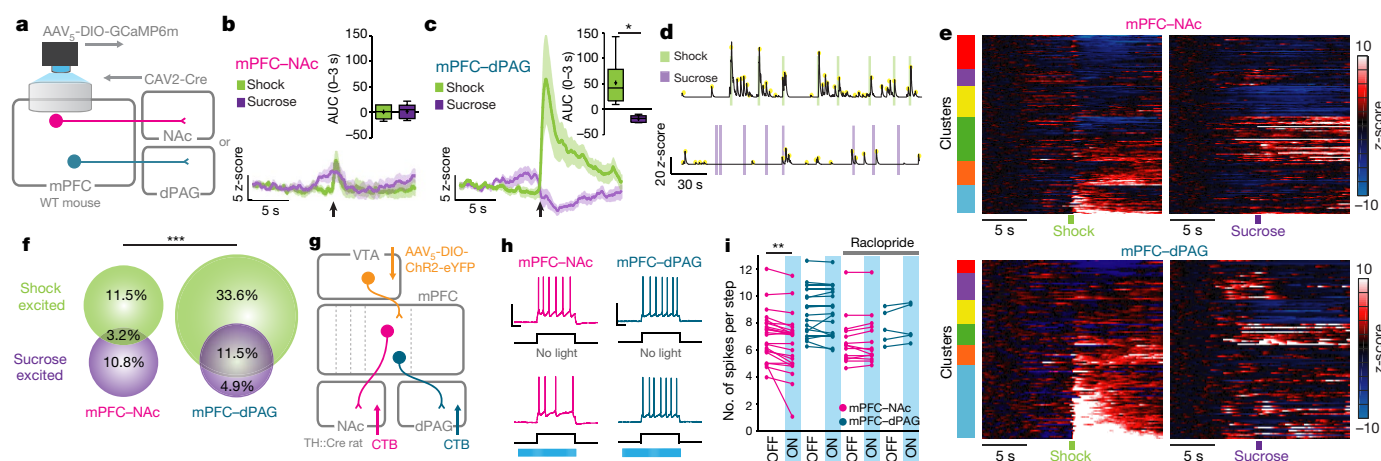
Fig. 3 | mPFC–dPAG neurons preferentially respond to aversive stimuli. a, Strategy for recording calcium activity in mPFC–dPAG and mPFC–NAc neurons in wild-type mice. **b**, Bulk fluorescence aligned to shock and sucrose bout in mice expressing GCaMP6m in mPFC–NAc neurons (mPFC–NAc::GCaMP6m mice) ($n = 5$ mice). Responses to sucrose did not differ from responses to shock (0–3 s AUC) in these mice. Two-tailed paired t-test, $t_4 = 0.1482$, $P = 0.8893$. AUC, area under the curve. **c**, Bulk fluorescence in mPFC–dPAG::GCaMP6m neurons ($n = 6$ mice). Calcium responses to shock were greater than responses to sucrose (0–3 s AUC). Two-tailed paired t-test, $t_5 = 3.743$, $*P = 0.0134$. **d**, Signals were extracted from individual regions of interest (ROIs). Individual transients indicated by yellow dots. **e**, Average traces per ROI aligned to shock or sucrose for each population. Agglomerative clustering results are shown in the bars on the left of each heat map. **f**, The distribution of shock- and sucrose-excited cells for mPFC–dPAG::GCaMP6m ($n = 118$ ROIs) was different from that

for mPFC–NAc::GCaMP6m ($n = 169$ ROIs) ($\chi^2 = 14.76$, $***P = 0.0006$). **g**, Strategy for manipulation of VTA^{DA}–mPFC::ChR2 and recording from dPAG or NAc projectors ex vivo. **h**, Representative traces from mPFC–NAc and mPFC–dPAG neurons during a current step without and with activation of VTA^{DA}–mPFC (470 nm, 20 Hz, 60 pulses). **i**, Optical activation of VTA^{DA}–mPFC did not influence mPFC–dPAG neurons ($n = 17$ cells), but decreased the number of spikes per step in mPFC–NAc neurons ($n = 24$ cells), an effect not observed upon treatment with raclopride (a D2-type dopamine-receptor antagonist) (mPFC–dPAG, $n = 5$ cells; mPFC–NAc, $n = 14$ cells). Two-tailed repeated measures ANOVA, $F_{3,56} = 5.331$, $P = 0.0027$, Bonferroni multiple comparisons tests, mPFC–NAc OFF versus mPFC–NAc ON, $**P < 0.001$. Shading represents s.e.m., boxes show median, first and third quartiles, points indicate the mean and whiskers show minimum and maximum (**b**, **c**). Scale bars (electrophysiology): x axis, 500 ms; y axis, 50 mV.
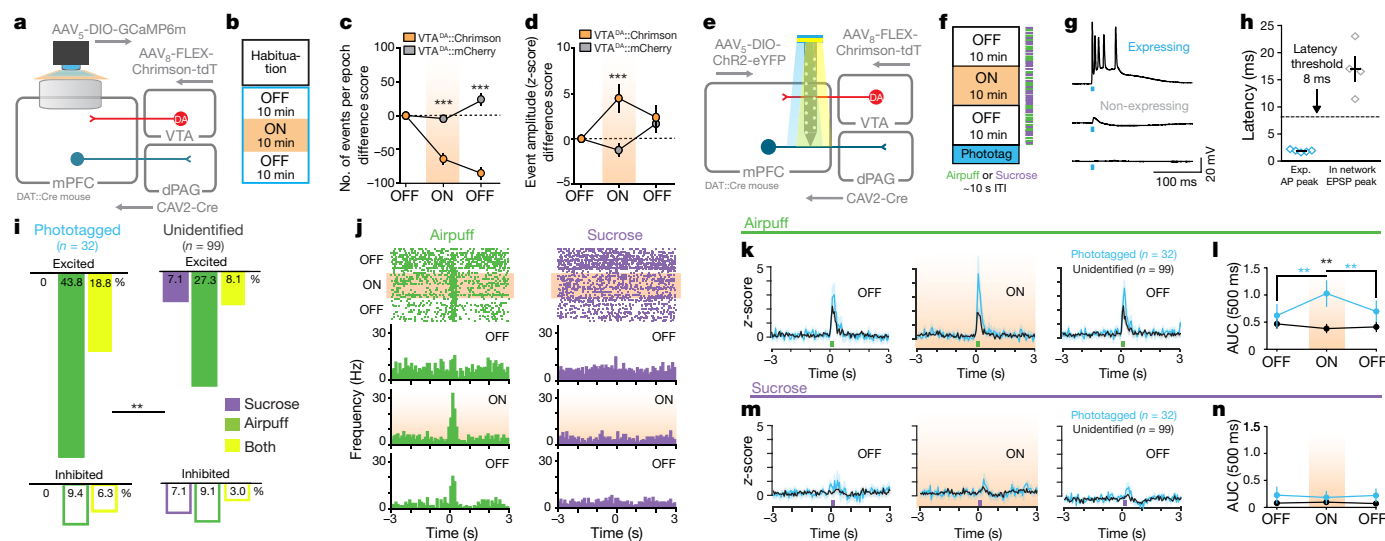

Fig. 4 | Dopamine enhances the SNR of mPFC–dPAG neural responses to aversive stimuli. a, Strategy for imaging activity in mPFC–dPAG::GCaMP6m neurons and activation of VTA^{DA}–mPFC in vivo ($n = 3$ mice, 5 recording sessions). **b**, During the ON epoch, VTA^{DA}–mPFC::Chrimson terminals were stimulated with 590-nm light (20 Hz, 60 pulses, every 30 s). **c**, Stimulation of VTA^{DA}–mPFC terminals decreased event frequency (Chrimson, $n = 4$ mice, 44 ROIs; mCherry control, $n = 5$ mice, 50 ROIs). Two-way repeated measure ANOVA, $F_{2,184} = 57.61$, $P < 0.0001$; Bonferroni multiple comparisons tests, $***P < 0.0001$. **d**, VTA^{DA}–mPFC stimulation increased event amplitude. Two-way repeated measure ANOVA, $F_{2,184} = 5.843$, $P = 0.0035$; Bonferroni multiple comparisons tests, $***P < 0.0001$. **e**, Strategy for manipulation of VTA^{DA}–mPFC and identification of mPFC–dPAG::ChR2 using in vivo electrophysiology. **f**, During the ON epoch, VTA^{DA}–mPFC::Chrimson were stimulated with 593-nm light (20 Hz, 60 pulses, every 30 s). Mice received random sucrose and airpuff deliveries. ITI, inter-trial interval. **g**, Representative traces from ChR2-expressing and non-ChR2-expressing

neurons in response to blue light ex vivo. **h**, Latency to action potential (AP) peak for ChR2-expressing ($n = 5$ cells) and to excitatory postsynaptic potential (EPSP) peak for non-ChR2-expressing ($n = 4$ cells) neurons. **i**, Excitatory response patterns were different between populations ($\chi^2 = 9.52$, $P = 0.0016$). **j**, Representative peri-stimulus time histogram (PSTH) of mPFC–dPAG neurons. **k**, Population z-score for phototagged and unidentified units aligned to airpuff. **l**, Stimulation of VTA^{DA}–mPFC neurons enhanced airpuff responses in phototagged, but not unidentified neurons. Two-way repeated measure ANOVA, $F_{2,258} = 6.196$, $P = 0.0024$; Bonferroni multiple comparisons tests, phototagged OFF1 versus ON, $**P = 0.0014$; phototagged ON versus OFF2, $**P = 0.0091$; unidentified OFF1 versus ON versus OFF2, $P > 0.05$; phototagged ON versus unidentified ON, $**P = 0.0012$. **m**, Population z-score for phototagged and unidentified units aligned to sucrose. **n**, VTA^{DA}–mPFC did not change responses to sucrose. Two-way repeated measure ANOVA, $F_{2,258} = 0.4420$, $P = 0.6432$. Error bars (**c**, **d**, **h**, **l**, **n**) and shading (**k**, **m**) represent s.e.m.

each population, mPFC–NAc responses were heterogeneous while mPFC–dPAG responses were robustly biased towards shock (Fig. 3f and Supplementary Videos 4, 5). Further, transients in mPFC–dPAG neurons were both more frequent and higher in amplitude during shock sessions, compared to those in mPFC–NAc neurons (Extended Data Fig. 6).

On the basis of these functional and anatomical differences, we next sought to assess the impact of dopamine on mPFC–NAc and mPFC–dPAG neurons. To test whether dopamine had different effects on the intrinsic excitability of these populations, we performed whole-cell patch-clamp recordings in acute slice preparations of the mPFC containing VTA[DA]–mPFC terminals expressing ChR2 and retrogradely labelled mPFC–dPAG or mPFC–NAc neurons (Fig. 3g). We delivered current steps to evoke intermediate levels of neural firing that were paired with photostimulation of VTA[DA]–mPFC neurons on interleaved sweeps (Fig. 3h). Photostimulation of VTA[DA]–mPFC neurons reduced the number of spikes per step for mPFC–NAc neurons, but did not detectably alter the excitability of mPFC–dPAG neurons (Fig. 3i). Dopamine-mediated suppression of mPFC–NAc neurons was blocked by the D2-type dopamine receptor antagonist raclopride (Fig. 3i). To investigate dopamine receptor localization on mPFC–NAc and mPFC–dPAG neurons, we performed retrograde labelling of projectors in Drd1a-Cre and Drd2-Cre mice injected with adeno-associated virus (AAV) for Cre-dependent expression of eYFP. We found that mPFC–NAc projectors expressed both D1 and D2 dopamine receptors, whereas mPFC–dPAG projectors largely did not express them (Extended Data Fig. 7). Since dopamine did not modulate mPFC–dPAG neurons ex vivo and this population did not robustly express dopamine receptors, we considered the possibility that dopamine modulates the SNR of incoming sensory information—a function that is only revealed when such inputs are intact.

To investigate this idea, we simultaneously recorded calcium dynamics in mPFC–dPAG neurons while stimulating VTA[DA] terminals in vivo. Expression of the fluorescent calcium sensor GCaMP6m was targeted to mPFC–dPAG neurons, and dopamine neurons were transduced with the depolarizing red-shifted opsin Chrimson[29] or mCherry using a dopamine transporter (DAT)::Cre mouse (Fig. 4a). VTA[DA]–mPFC terminals were activated during a 10-min 'laser-ON' epoch, flanked by two 'laser-OFF' epochs without photostimulation (Fig. 4b). Consistent with the model in which dopamine increases the SNR of mPFC–dPAG activity, VTA[DA]–mPFC stimulation decreased calcium event frequency (Fig. 4c and Extended Data Fig. 8) and increased event amplitude (Fig. 4d and Extended Data Fig. 8). To demonstrate alterations in the SNR, we next explored how dopamine altered activity in mPFC–dPAG neurons in the presence of aversive signals. To test this, we used ChR2-assisted photoidentification of mPFC–dPAG projectors during electrophysiological recordings, coupled with optical manipulations of VTA[DA]–mPFC (Fig. 4e). VTA[DA]–mPFC terminals were stimulated during a 10-min 'laser-ON' epoch flanked by two 'laser-OFF' epochs in an awake, in vivo head-fixed preparation[30]. During recording, unpredicted sucrose and airpuff presentations were interleaved and mPFC–dPAG neurons expressing ChR2 were optically tagged with blue light at the end of the session (Fig. 4f). Of the 204 total mPFC units recorded, 32 were photoidentified as mPFC–dPAG projectors using an ex vivo verified photoresponse latency threshold (Fig. 4 g, h). Consistent with our results from in vivo calcium imaging, a large proportion of mPFC–dPAG neurons were excited by airpuff (Fig. 4i). Stimulation of VTA[DA]–mPFC terminals did not change basal firing rates in phototagged or unidentified populations (Extended Data Fig. 9). Examination of time-locked neural activity revealed a selective dopamine-mediated amplification of airpuff responses (Fig. 4j–l), but not sucrose responses (Fig. 4m, n) in mPFC–dPAG neurons. This increase in SNR was not observed in the unidentified or photoinhibited populations (Extended Data Fig. 10).

Threatening environmental stimuli require immediate disengagement from ongoing behaviour and engagement of escape and avoidance strategies, which requires tuning of valence-defined circuits. We speculate that dopamine in the mPFC primes top-down neural circuits that encode aversive stimuli in order to promote avoidance and escape-related defensive behaviours. These findings have clinical relevance to neuropsychiatric disorders characterized by dopamine dysregulation in the mPFC. Our data suggest that mesocortical dopamine governs information routing down discrete mPFC projections and highlights the need for targeted circuit-specific dopamine therapies in the mPFC.

Online content

1. Arnsten, A. F. T. Stress signalling pathways that impair prefrontal cortex structure and function. *Nat. Rev. Neurosci.* **10**, 410–422 (2009).
2. Miller, E. K. & Cohen, J. D. An integrative theory of prefrontal cortex function. *Annu. Rev. Neurosci.* **24**, 167–202 (2001).
3. Cohen, J. D., Braver, T. S. & Brown, J. W. Computational perspectives on dopamine function in prefrontal cortex. *Curr. Opin. Neurobiol.* **12**, 223–229 (2002).
4. Kroener, S., Chandler, L. J., Phillips, P. E. M. & Seamans, J. K. Dopamine modulates persistent synaptic activity and enhances the signal-to-noise ratio in the prefrontal cortex. *PLoS ONE* **4**, e6507 (2009).
5. Rolls, E. T., Loh, M., Deco, G. & Winterer, G. Computational models of schizophrenia and dopamine modulation in the prefrontal cortex. *Nat. Rev. Neurosci.* **9**, 696–709 (2008).
6. Winterer, G. & Weinberger, D. R. Genes, dopamine and cortical signal-to-noise ratio in schizophrenia. *Trends Neurosci.* **27**, 683–690 (2004).
7. Popescu, A. T., Zhou, M. R. & Poo, M.-M. Phasic dopamine release in the medial prefrontal cortex enhances stimulus discrimination. *Proc. Natl Acad. Sci. USA* **113**, E3169–E3176 (2016).
8. Noudoost, B. & Moore, T. Control of visual cortical signals by prefrontal dopamine. *Nature* **474**, 372–375 (2011).
9. Williams, G. V. & Goldman-Rakic, P. S. Modulation of memory fields by dopamine D1 receptors in prefrontal cortex. *Nature* **376**, 572–575 (1995).
10. Burgos-Robles, A. et al. Amygdala inputs to prefrontal cortex guide behavior amid conflicting cues of reward and punishment. *Nat. Neurosci.* **20**, 824–835 (2017).
11. Euston, D. R., Gruber, A. J. & McNaughton, B. L. The role of medial prefrontal cortex in memory and decision making. *Neuron* **76**, 1057–1070 (2012).
12. Kim, C. K. et al. Simultaneous fast measurement of circuit dynamics at multiple sites across the mammalian brain. *Nat. Methods* **13**, 325–328 (2016).
13. Lammel, S., Ion, D. I., Roeper, J. & Malenka, R. C. Projection-specific modulation of dopamine neuron synapses by aversive and rewarding stimuli. *Neuron* **70**, 855–862 (2011).
14. Abercrombie, E. D., Keefe, K. A., DiFrischia, D. S. & Zigmond, M. J. Differential effect of stress on in vivo dopamine release in striatum, nucleus accumbens, and medial frontal cortex. *J. Neurochem.* **52**, 1655–1658 (1989).
15. Thierry, A. M., Tassin, J. P., Blanc, G. & Glowinski, J. Selective activation of mesocortical DA system by stress. *Nature* **263**, 242–244 (1976).
16. Mantz, J., Thierry, A. M. & Glowinski, J. Effect of noxious tail pinch on the discharge rate of mesocortical and mesolimbic dopamine neurons: selective activation of the mesocortical system. *Brain Res.* **476**, 377–381 (1989).
17. Finlay, J. M., Zigmond, M. J. & Abercrombie, E. D. Increased dopamine and norepinephrine release in medial prefrontal cortex induced by acute and chronic stress: effects of diazepam. *Neuroscience* **64**, 619–628 (1995).
18. Heien, M. L. A. V., Phillips, P. E. M., Stuber, G. D., Seipel, A. T. & Wightman, R. M. Overoxidation of carbon-fiber microelectrodes enhances dopamine adsorption and increases sensitivity. *Analyst* **128**, 1413–1419 (2003).
19. Bandler, R. & Carrive, P. Integrated defence reaction elicited by excitatory amino acid microinjection in the midbrain periaqueductal grey region of the unrestrained cat. *Brain Res.* **439**, 95–106 (1988).
20. Deng, H., Xiao, X. & Wang, Z. Periaqueductal gray neuronal activities underlie different aspects of defensive behaviors. *J. Neurosci.* **36**, 7580–7588 (2016).
21. Tovote, P. et al. Midbrain circuits for defensive behaviour. *Nature* **534**, 206–212 (2016).
22. Franklin, T. B. et al. Prefrontal cortical control of a brainstem social behavior circuit. *Nat. Neurosci.* **20**, 260–270 (2017).
23. Murugan, M. et al. Combined social and spatial coding in a descending projection from the prefrontal cortex. *Cell* **171**, 1663–1677 (2017).
24. Otis, J. M. et al. Prefrontal cortex output circuits guide reward seeking through divergent cue encoding. *Nature* **543**, 103–107 (2017).
25. Britt, J. P. et al. Synaptic and behavioral profile of multiple glutamatergic inputs to the nucleus accumbens. *Neuron* **76**, 790–803 (2012).
26. Ghosh, K. K. et al. Miniaturized integration of a fluorescence microscope. *Nat. Methods* **8**, 871–878 (2011).
27. Chen, T.-W. et al. Ultrasensitive fluorescent proteins for imaging neuronal activity. *Nature* **499**, 295–300 (2013).
28. Zhou, P. et al. Efficient and accurate extraction of in vivo calcium signals from microendoscopic video data. *eLife* **7**, e28728 (2018).

29. Klapoetke, N. C. et al. Independent optical excitation of distinct neural populations. *Nat. Methods* **11**, 338–346 (2014).
30. Beyeler, A. et al. Divergent routing of positive and negative information from the amygdala during memory retrieval. *Neuron* **90**, 348–361 (2016).

METHODS

Surgery and viral injections. Specific details of subjects and surgery for each experiment are provided below. All surgery was performed under aseptic conditions and body temperature was maintained with a heating pad. Rodents were anaesthetized with isoflurane mixed with oxygen (5% for induction, 2–2.5% for maintenance, 1 l min^{-1} oxygen flow rate) and placed in a digital small-animal stereotaxic instrument (David Kopf Instruments). Following initial induction, hair was removed from the dorsal surface of the head with hair clippers, ophthalmic ointment was applied to the eyes, the incision area was scrubbed with alcohol pads and betadine ($3\times$ each), and 2% lidocaine was injected just under the skin surface above the skull for topical anaesthesia. All measurements were made relative to bregma (unless noted otherwise) for virus/implant surgeries. Viral injections were performed using a beveled microinjection needle (26 gauge for rats; 33 gauge for mice) with a 10 µl microsyringe (Nanofil; WPI) delivering virus at a rate of 0.05–0.01 µl min^{-1} using a microsyringe pump (UMP3; WPI) and controller (Micro4; WPI). For injections at multiple locations on the dorsal–ventral axis, the most ventral location was completed first and the injection needle was immediately relocated to the more dorsal location for the next injection. After completion of injection, 15 min were allowed to pass before the needle was slowly withdrawn. After viral infusions were completed, craniotomies were filled with bone wax and the incision closed with nylon sutures. Subjects were maintained under a heat lamp and provided 0.05 mg kg^{-1} (rat) or 0.10 mg kg^{-1} (mouse) buprenorphine (subcutaneously, diluted in warm Ringer's solution) until fully recovered from anaesthesia.

All experiments involving the use of animals were in accordance with NIH guidelines and approved by the MIT Institutional Animal Care and Use Committee. For all experiments involving viral or tracer injections, animals containing mistargeted injection(s) were excluded after histological verification.

Viral constructs. Recombinant adeno-associated virus serotype 5 (AAV$_5$) vectors containing coding sequences for ChR2[31,32], NpHR[33,34], or fluorescent proteins (mCherry or eYFP) were packaged by the University of North Carolina Vector Core (Chapel Hill, NC). AAV$_8$-hSyn-FLEX-ChrimsonR-tdTomato[29] and AAV$_5$-hSyn-mCherry were packaged by the University of North Carolina Vector Core (Chapel Hill, NC). Viruses carrying GCaMP6m[27,35] were packaged by the University of Pennsylvania Vector Core (Philadelphia, PA). Canine adeno-associated virus[36] carrying Cre recombinase (CAV2-Cre 4.2×10^{12} infectious units per ml) was packaged and obtained from E. Kremer (Institut de Génétique Moléculaire de Montpellier, France). AAV$_9$-hEF1a-DIO-synaptophysin-mCherry was obtained from R. Neve (Viral Gene Transfer Core Facility, MIT, now located at Massachusetts General Hospital).

Catecholamine terminal tracing. Male heterozygous tyrosine hydroxylase (TH)::Cre mice (8–9 weeks old) received unilateral injections of the anterograde-travelling AAV$_5$ encoding the fluorescent protein mCherry or eYFP under a double-floxed inverted open-reading frame (DIO) construct (AAV$_5$-EF1a-DIO-mCherry or AAV$_5$-EF1a-DIO-eYFP) in the ventral tegmental area (VTA; AP: -3.4, ML: $+0.4$, DV: -4.25 (1 µl)) and locus coeruleus (LC; AP: -5.45, ML: 1.25, DV: -4.0 and -7.8 (0.5 µl)), counterbalanced. Mice ($n = 3$) were given 10 weeks for viral expression and trafficking of the fluorescent protein to terminals in the medial prefrontal cortex (mPFC). After virus incubation, mice were transcardially perfused, and tissue was sectioned and prepared for immunohistochemistry to label TH$^+$ neurons for histological analyses (described below). For quantification of fluorescently labelled TH$^+$ neurons in the LC and VTA, single z-stacks in the medial ventral tegmental area (VTA) and central LC were acquired using a scanning confocal microscope (Olympus FV1000) with Fluoview software (Olympus) under a $60\times/1.42$ numerical aperture (NA) oil-immersion objective. The number of co-labelled (TH$^+$ and eYFP/mCherry$^+$) neurons and eYFP/mCherry-only labelled neurons were counted. z-stack stitches encompassing both prelimbic (PL) and infralimbic (IL) regions of the mPFC were acquired under a $40\times/1.30$-NA oil-immersion objective. Quantification of fluorescence intensity as a proxy for terminal density was accomplished by analysing 100 (w) $\times$ 200 (h) µm sections across mPFC layers based on DAPI density/morphology in Fiji[37]. Sections were normalized to the section with peak fluorescence within subjects. Sample size was based on reports in related literature and was not predetermined by calculation.

Fast-scan cyclic voltammetry. *Subjects.* For FSCV, male and female heterozygous BAC transgenic TH::Cre rats[38] ($\sim$220 g body weight) were dual housed with ad libitum access to water on a normal 12:12-h light:dark cycle (lights on at 09:00). *Surgery.* TH::Cre rats, which had received a unilateral injection of 2 µl AAV$_5$ encoding ChR2–mCherry or halorhodopsin 3.0 (NpHR)–eYFP, under a double-floxed inverted open-reading frame construct (AAV$_5$-EF1a-DIO-ChR2-mCherry or AAV$_5$-EF1a-DIO-NpHR-eYFP) in the VTA (AP: -5.3, ML: $+0.7$, DV: -8.2 and -7.8 (1 µl each)) were given at least 8 weeks for viral expression before recording. In vivo FSCV experiments were conducted similar to those previously described[39,40]. Rats were anaesthetized with urethane (1.5 g kg^{-1}, intraperitoneally) diluted in sterile saline and placed in a stereotaxic frame located in a Faraday cage. For both experiments, a glass-encased carbon fibre electrode ($\sim$120 µm exposed

carbon fibre, epoxied seal) was lowered into the mPFC (AP: $+3.2$, ML: $+0.8$ mm relative to bregma; DV: -2.0 mm from brain surface) through a small craniotomy performed above the deep layers of the mPFC for voltammetric recordings.

For ChR2 experiments ($n = 5$), additional craniotomies were performed above the VTA (AP: -5.5, ML: -0.6 mm), LC (AP: -9.75, ML: -1.25 mm), and contralateral cortex. An Ag/AgCl reference electrode, chlorinated just beforehand, was implanted in the contralateral cortex. A manually constructed optical fibre[41] (400-µm core, 0.48 NA; Thorlabs) cut to 8 mm in length, held in a 2.5 mm ferrule (Precision Fibre Products), was implanted above the VTA (DV: -7.0 mm), and a 26-gauge guide cannula (PlasticsOne) was positioned over the LC (DV: -6.6 mm). Implants were secured to the skull with adhesive cement (C&B Metabond; Parkell).

After the cement dried, the optic fibre implant was connected to a patch cable (Doric) via a ceramic sleeve (PFP) and both reference and carbon-fibre recording electrode were connected to the FSCV interface via a custom-made head stage (S. Ng-Evans, P. E. M. Phillips Laboratory, University of Washington). Dopamine release was evoked by optical activation of the VTA using 150 pulses of 473-nm light (25 mW, 5-ms pulse duration) at 50 or 30 Hz, delivered via a diode-pumped solid state (DPSS) laser (OEM Laser Systems) through the attached patch cable and controlled using a Master-8 pulse stimulator (A.M.P.I.). Electrodes were stereotaxically lowered in 0.2-mm increments until optimal dopamine release was detected by photoactivation of VTA dopamine neurons. Optically evoked dopamine release was not detected from one subject for unknown reasons; however, tail-pinch-evoked catecholamine release was observed with characteristic cyclic voltammograms (CVs) for catecholamines, and therefore this rat was included in analyses.

For NpHR experiments ($n = 5$), craniotomies (in addition to that above the mPFC) were performed above the VTA (AP: -5.5, ML: -0.6 mm), nucleus accumbens shell (NAc, AP: 1.5, ML: $+0.9$), and contralateral cortex. An Ag/AgCl reference electrode, chlorinated just beforehand, was implanted in the contralateral cortex and secured to the skull with adhesive cement (C&B Metabond; Parkell). After the cement dried, reference and carbon-fibre recording electrodes were connected to an FSCV interface via a head stage and the recording electrode was stereotaxically lowered into the NAc shell (DV: -6.6 mm relative to brain surface). Following equilibration (see below), a combination bipolar electrical stimulation electrode and 26-gauge guide cannula (PlasticsOne) was stereotaxically lowered above the VTA (DV: -6.5 mm) in 0.2-mm increments until dopamine release was detected in the NAc by electrical activation of VTA dopamine neurons via 60 Hz, 60 pulses (biphasic, 200 µA), controlled by an ISO-Flex stimulus isolator (A.M.P.I.). Following dopamine detection, the combination electrical stimulation–guide cannula electrode was cemented in place (C&B Metabond; Parkell) slightly dorsal of the VTA, and the carbon-fibre recording electrode transferred into the mPFC (DV: -2.0 mm) and allowed to equilibrate. Sample sizes were based on reports in related literature and were not predetermined by calculation.

Data acquisition. For both experiments, electrodes were allowed to equilibrate for 20 min at 60 Hz and 10 min at 10 Hz. Voltammetric recordings were collected at 10 Hz by applying a triangular waveform (-0.4 V to $+1.3$ V to -0.4 V, 400 V s^{-1}) to the carbon-fibre electrode versus the Ag/AgCl reference implanted in the contralateral cortex[42]. Data were collected in 60-s files with the tail-pinch onset occurring 10 s into the file for a duration of 10 s (TarHeelCV). Files were collected every 120 s and background subtracted at the lowest current value before pinch onset. Evoked signals maintained characteristic CVs for dopamine and noradrenaline[18], with oxidation and reduction peaks at $\sim$+0.65 V and $\sim$−0.2 V, respectively. For ChR2 experiments, five tail-pinch recordings were obtained with a 120-s inter-recording interval, before LC inactivation. After recordings were completed, 1 µl of tetrodotoxin (TTX, 10 ng per 1.5 µl artificial cerebral spinal fluid) mixed with Fast Green (for spread visualization) was injected into the LC via a microinjection needle through the 26-gauge guide cannula controlled by a syringe pump. Two minutes following infusion completion, five tail-pinch recordings were obtained with a 120-s inter-recording interval, post-LC inactivation. For NpHR experiments, recordings were similarly obtained as 10 recordings at 120-s inter-recording interval. Trials were interleaved with no optical manipulation trials (OFF trials) and trials in which VTA dopamine neurons were inhibited with 20 s constant 598-nm DPSS laser light (5 mW) delivered by a stripped 200 µm core patch cable (Doric) inserted into the combination electrical stimulation/guide cannula located dorsal of the NpHR-expressing VTA dopamine neurons (ON trials). Optical inhibition was initiated 5 s into each ON trial (that is, 5 s before tail-pinch onset) and remained for 20 s (that is, ending 5 s after tail-pinch offset). Oscillatory signals were often observed in the mPFC (however, no such signals were detected in the NAc) and were attenuated by tail pinch and electrical stimulation. Trial averaging alleviated oscillatory interference. Following recording, rats were transcardially perfused and fixed (as described below) and processed using immunohistochemistry for TH immunolabelling to confirm viral expression and implant/recording electrode locations using confocal microscopy. Spread of TTX–Fast Green was recorded during tissue sectioning on a freezing, sliding microtome.

Data analysis. Signals were converted to changes in catecholamine concentration using chemometric, principal component regression, and residual analyses using a custom LabView program (Umich CV, courtesy of R. Keithley), as previously described[43,44] using in vivo optically and electrically evoked CVs and calibration data obtained from an average of 10 electrodes calibrated in known dopamine concentrations and pH units as previously described[17]. For quantification of blue-light-evoked dopamine, AUC was calculated during the 5-s pre-stimulation period, compared to the AUC 5 s following the initiation of 20-Hz, 60 pulses laser light. For quantification of tail-pinch-evoked dopamine, AUC was calculated during the 10 s before pinch onset, compared to the AUC during the 10 s following pinch onset. For comparison of pinch-evoked signals in ON and OFF trials in NpHR experiments, AUC was calculated during the 30-s period following pinch onset.

VTA[DA]–mPFC behavioural optogenetic experiments. *Subjects.* Male heterozygous BAC transgenic TH::Cre rats[38] ($\sim$220 g) were dual housed with ad libitum access to water on a normal 12:12 h light:dark cycle (lights on at 09:00). About 1 week following viral injection surgeries, rats were individually housed with restricted food access ($\sim$16–20 g chow per day) for $\sim$10 weeks, but retained ad libitum access to water. Sample size was based on reports in related literature and was not predetermined by calculation.

Surgery. TH::Cre rats that had received a unilateral injection of 2 µl AAV$_5$-EF1a-DIO-ChR2-eYFP ($n = 6$–8) or AAV$_5$-EF1a-DIO-eYFP ($n = 5$–7) in the VTA (AP: -5.3, ML: $+0.7$, DV: -8.2 and -7.8 (1 µl each)) were given at least 12 weeks to ensure Cre-specific viral transduction of ChR2 in VTA[DA] neurons and protein transport to distal terminals in the mPFC. Following incubation, 20G stainless steel cannulae (PlasticsOne) were bilaterally implanted above the mPFC (AP: $+3.2$–3.6; ML: ± 2.0, DV: -2.8; mm relative to bregma at a 15° angle, bilateral). Guide cannulae were secured to the skull with 2–4 skull screws, a layer of adhesive cement (C&B Metabond; Parkell), followed by black cranioplastic cement (Ortho-Jet; Lang) containing gentamicin antibiotic. The implant was allowed to dry completely before closure of the incision with nylon sutures. Dummies (24G cannulae) were inserted into the guide cannulae to prevent clogging.

General testing procedures. On each test day, a 400-µm core optical fibre was inserted and attached to the cannulae. Optical fibres extended $\sim$250–500-µm beyond the cannulae tips. Rats were then transferred to their behavioural apparatus and connected to patch cords connected to dual-rotating commutators for testing. Real-time place preference/aversion and conditioned place preference/aversion assays were identical to those described below. Laser light (473 nm) was delivered through the patch cords at 20 Hz, 60 pulses of 5 ms, every 30 s at 20 mW from optic fibre tip. If an optic fibre broke into a guide cannula or if a guide cannula became clogged, the contralateral guide cannula was used for the remaining experiments. Manipulated hemispheres were counterbalanced.

Real-time place preference/aversion. Individual food-restricted rats were placed in a Plexiglas arena (24 in (l) × 24 in (w) × 20 in (h)) and were allowed to move freely between two compartments for 1 h in a dimly lit room containing constant white noise (Marpac Dohm-DS dual speed sound conditioner). Entry into one half of the chamber resulted in photostimulation (VTA[DA]–mPFC::ChR2/eYFP, unilateral 20 Hz, 60 pulses of 5 ms every 30 s, 20 mW; mPFC–dPAG/NAc::ChR2/eYFP, bilateral 20 Hz 5-ms pulses, 12–15 mW, see below). Stimulation and no-stimulation sides were counterbalanced between animals. Rats were tested on two consecutive days, and on the second day the stimulation side and no stimulation side were reversed. A video camera positioned directly above the arena tracked and recorded movement using EthoVision XT (Noldus). All data presented are tracked from the 'centre' of the subject and time spent in each zone was averaged across the two testing sessions. In between subjects, the behavioural chamber was thoroughly cleaned with 10% glass cleanser diluted in double-distilled water (ddH$_2$O).

Conditioned place preference/aversion. Individual food-restricted rats were placed in a Plexiglass arena (30 in (l) × 15 in (w) × 25 in (h)) divided into two compartments: one with vertical stripes and the other with horizontal stripes. On day 1 (habituation), rats were allowed to move freely between the two compartments for 15 min in a brightly lit room containing constant white noise (Marpac Dohm-DS dual speed sound conditioner). Movement was tracked by an overhead video camera positioned above the arena and time spent in each compartment was calculated using EthoVision XT (Noldus). On days 2 and 3, rats were exposed to conditioning sessions (20 min each, 1 per day) during which they were confined to one side of the chamber and received optical stimulation (VTA[DA]–mPFC::ChR2/eYFP = unilateral 20 Hz, 60 pulses of 5 ms every 30 s, 20 mW; mPFC–dPAG/NAc::ChR2/eYFP = bilateral 20 Hz 5-ms pulses, 12–15 mW, see below) or no stimulation (counterbalanced for order and side across animals). On day 4 (test), rats were placed in the chamber and allowed to freely explore both compartments in the absence of optical stimulation. Again, movement was tracked by an overhead video camera positioned above the arena using EthoVision XT (Noldus) and a time difference score was calculated by subtracting the time spent in the stimulation-paired compartment on the habituation day from the time spent in the stimulation-paired compartment on the test day (test(time spent in paired side) − habituation(time spent in paired side)).

Stimulus competition task. Training and testing procedures were similar to those previously described[10]. Training was performed in standard rat operant chambers (23 × 30 × 40 cm; Med Associates) located within sound-attenuating cubicles. Each chamber was equipped with a red house light, speakers for the delivery of tone cues, a sucrose port that was equipped with an infrared beam for the detection of port entries and exits, a syringe pump to deliver sucrose (30% in cage water), two light cues on either side of the sucrose port, and a grid floor for the delivery of electrical shocks. Chambers were wiped down with 70% isopropyl alcohol after each session. Before training, rats were pre-exposed to sucrose in their home cage and were magazine trained in the operant boxes (60 min, 20 sucrose deliveries). The first phase of training consisted of Pavlovian reward conditioning in which rats learned to associate a 20-s conditioned stimulus (CS[suc], either a light cue or tone cue (5 kHz, 80 dB), counterbalanced between subjects) with sucrose delivery into the reward port (30% sucrose, 120 µl per trial). Sucrose was delivered over 10 s during the cue presentation (5–15 s, relative to CS[suc] onset). ITIs were set to an average of 60 s. If sucrose was not consumed (as detected by the lack of a port entry during the 20-s CS[suc] presentation), sucrose was immediately removed after cue offset via activation of a vacuum tube located in the sucrose port. Rats were trained on sucrose conditioning for 3 days, with each session comprising 25 trials delivered over $\sim$35 min. The second phase of training consisted of four Pavlovian discrimination sessions where conditioned stimuli predicted sucrose (CS[suc]) or footshock (CS[shk]) delivery. During these sessions, the opposite conditioned stimulus (either a light cue or tone cue (5 kHz, 80 dB)) co-terminated with 0.5-s footshock (0.60 mA, 19.5–20 s relative to CS[shk] onset). CS[suc] and CS[shk] cues were counterbalanced and presented in a pseudorandom manner. Each session consisted of 40 total trials (20 of each trial type) with a variable $\sim$60-s ITI. During sucrose conditioning and discrimination sessions, animals were unilaterally connected to a rotating commutator via a dummy patch cord, but no laser light was delivered.

The third phase was the stimulus competition test sessions. Before these sessions, an optical fibre was loaded into a guide cannula, connected to a patch cord, and attached to a rotating commutator, identical to the previous phases. During competition sessions, in addition to CS[suc] and CS[shk] trials, competition trials were introduced—in which CS[suc] and CS[shk] cues and their respective outcomes were co-presented to evoke conflicting motivation between reward- and fear-associated behaviours. One second before competition trials (CS[comp]), the 473-nm laser was triggered (20 Hz, 60 pulses of 5 ms every 5 s) for the duration of the 20-s compound cue (4 stimulation trains per competition session). Each competition session consisted of 60 total trials (20 of each trial type) with a variable $\sim$60-s ITI.

Data analysis. Sucrose port entries and exits provided a read-out for reward-related behaviour (based on the percentage of time in the port during each trial type) and were sampled from infrared beam breaks (Med-PC IV, Med Associates. Freezing, defined as the lack of all movement other than respiration, provided a read-out for aversively motivated behaviour. Videos were sampled using side-profiled infrared cameras at 30 frames per second and freezing was quantified using an automated custom MATLAB script that calculated frame-by-frame changes in total pixel intensity as an approximation for animal movement. Frame-by-frame motion values were converted into freezing scores using a binary method relative to a motion threshold. This method produced values which are highly correlated with hand-scored measurements of freezing[10]. The time spent in the port was subtracted from the freezing quantification, as animals showed little movement while collecting sucrose.

Retrograde cholera toxin-B tracing. *Rats.* Male wild-type Long–Evans rats ($\sim$220 g; Charles River Laboratories) were dual housed on a normal 12:12 h light:dark cycle (lights on at 09:00). Rats were prepared for stereotaxic surgery as described above using the viral infusion parameters also described above (under 'Surgery and viral injections'). In brief, 500 nl cholera toxin subunit B (CTB) conjugated to Alexa Fluor 488, 555 or 647[45] (0.1%, Molecular Probes) was injected into the dorsal periaqueductal grey (dPAG; AP: -6.6, ML: -0.6; DV: -5.4 mm) and NAc shell (AP: $+1.5$, ML: $+0.95$, DV: -7.5 mm) (colour counterbalanced between animals). After 7 days, rats were transcardially perfused and histologically prepared. z-stack stitches encompassing both prelimbic (PL) and intralimbic (IL) regions of the mPFC were acquired using a scanning confocal microscope (Olympus FV1000) with Fluoview software (Olympus) under a 40×/1.30-NA oil-immersion objective. Quantification of fluorescence intensity across layers was accomplished by analysing 200 (w) × 400 (h)-µm sections encompassing ventral PL/dorsal IL across mPFC layers based on DAPI density/morphology in Fiji. Sections were normalized to the section with peak fluorescence within subjects. For cell quantification, the number of CTB-positive and double-positive neurons was counted in both the IL and PL subregions of the mPFC using FluoView software (Olympus). To examine potential projections from the VTA to the dPAG, 14 VTA sections were immunostained for tyrosine hydroxylase (TH) (see below) and z-stacks were captured under a 40×/1.30-NA oil-immersion objective. In each stack, 100 DAPI$^+$ cells were identified and the proportions of TH$^+$ and CTB$^+$ cells were counted. Sample size was based on reports in related literature and was not predetermined by calculation.

Mice. Adult male wild-type C56BL/6 mice (~10 weeks of age; Jackson Laboratory) were prepared similarly to methods described above. In brief, 350 nl CTB conjugated to Alexa Fluor 488, 555 or 647 (Molecular Probes) was injected into the dorsal periaqueductal grey (dPAG; AP: −4.2, ML: −0.5; DV: −2.4 mm) and NAc shell (AP: +1.0, ML: +0.75, DV: −4.5 mm) (colour counterbalanced between animals). Histological, imaging, and data analyses are the same as previously described.

Projection-specific behavioural optogenetic experiments. *mPFC–dPAG and mPFC–NAc subjects.* Male wild-type Long–Evans rats (~220 g; Charles River Laboratories) were dual housed on a normal 12:12 h light:dark cycle (lights on at 09:00). About 1 week following viral injection surgeries, rats were individually housed with restricted food access (~16–20 g chow per day) for ~10 weeks, but retained ad libitum access to water. Rats were maintained on food restriction unless noted otherwise.

Surgery. For projection-specific targeting for behavioural optogenetics, male wild-type Long–Evans rats were bilaterally injected with 1.2 µl AAV5-EF1a-DIO-ChR2(H134R)-eYFP in the mPFC at two locations along the dorsal-ventral axis (0.6 µl each) (AP: +3.2; ML: ±0.75; DV: −3.5 and −2.5; mm relative to bregma). To achieve projection-specific recombination, retrogradely travelling CAV2-Cre (4.2 × 10¹² infectious units per ml; Institut de Genetique Moleculaire de Montpellier, France) was bilaterally injected (0.6 µl each) in the dPAG (AP: −6.0; ML: ±0.6; DV: −5.2; mm relative to bregma (0.4 µl)), or NAc (AP: +1.4; ML: ±1.0; DV: −7.4; mm relative to bregma (0.5 µl)). A subset of mPFC–dPAG rats were co-injected with 0.1 µl AAV5-hSyn-mCherry to visualize virus spread. About 7 days following virus surgery, rats were individually housed and placed on food restriction. About 10 weeks later, manually constructed optic fibres (400 µm core, 0.48 NA) (Thorlabs) held in a 2.5-mm ferrule (Precision Fibre Products) were implanted directly above ChR2/eYFP-expressing mPFC neurons projecting to either the dPAG or NAc for projection-specific manipulations (AP: +3.2–3.6; ML: ± 1.5, DV: −2.8; mm relative to bregma at a 10° angle, bilateral).

For terminal manipulations, AAV5-CaMKIIa-ChR2-eYFP was bilaterally injected into the mPFC at two locations along the dorsal-ventral axis (0.6 µl each) (AP: +3.2; ML: ±0.75; DV: −3.5 and −2.5; mm relative to bregma). About 7 days following surgery, rats were individually housed and placed on food restriction. About 10 weeks later, manually constructed optic fibres (400-µm core, 0.48 NA) (Thorlabs, Newton) held in a 2.5 mm ferrule (Precision Fibre Products) were bilaterally implanted directly above the dPAG for mPFC terminal manipulations (AP: −6.6, ML: ±1.5; DV: −4.3 mm relative to bregma at a 10° angle, bilateral). For both experiments, optical fibres were secured to the skull with 2–4 skull screws, a layer of adhesive cement (C&B Metabond; Parkell), followed by black cranioplastic cement (Ortho-Jet; Lang) containing gentamicin antibiotic. The implant was allowed to completely dry before closure of the incision with nylon sutures.

Behavioural testing. Testing was performed at ~13 weeks following viral injection and ~10 days after optical-fibre implantation to allow sufficient time for transgene expression and tissue recovery. Throughout this period, rats were maintained on food restriction (~16–20 g chow per day). Rats were tested during their light phase (09:30–19:00) under food-deprived conditions. Optic fibre implants were connected to a 200-µm patch cable (Doric) using a ceramic sleeve (PFP), which connected to a bilateral commutator (rotary joint; Doric) by means of an FC/PC adaptor to allow unrestricted movement. A second patch cable, with an FC/PC connector at either end (Doric), connected the commutator to a 473-nm DPSS laser (OEM Laser Systems). A Master-8 pulse stimulator (A.M.P.I.) was used to control the output of the 473-nm laser, with a light power of ~10–15 mW (adjusted to account for optic fibre efficiency). Following each day's experimentation, rats were provided their ~16–20 g of standard chow after a variable 0.5–4 h window.

Open-field test. Individual food-restricted rats were placed in a Plexiglass arena (24 (l) × 24 (w) × 20 (h) in) and were allowed to move freely within the arena for 9 min with light stimulation occurring during the middle 3 min (3 min OFF, 3 min ON, 3 min OFF design) (mPFC–dPAG/NAc::ChR2/eYFP = bilateral 20 Hz 5-ms pulses, 12–15 mW). The room was brightly lit and contained constant white noise (Marpac Dohm-DS dual speed sound conditioner). A video camera positioned directly above the arena tracked and recorded movement using EthoVision XT (Noldus). In order to assess anxiety-related behaviour, the chamber was divided into a centre (40 × 40 cm) and periphery region. In between subjects, the behavioural chamber was thoroughly cleaned with 0.03% acetic acid diluted in ddH₂O. All data presented are tracked from the 'centre' of the subject.

Marble burying. Individual food-restricted rats were placed in a standard, rectangular rodent cage (33 (w) × 40 (l) × 20 (h) cm) containing ~7.5 cm of clean standard bedding and 16 black marbles, which was slightly elevated from the floor (1 m). Sixteen 1.3-cm diameter black marbles were placed on top of the even bedding in a 4 × 4 array separated from the cage sides by ~5 cm. Rats were tested across 2 days for 12 min each, counterbalanced for laser stimulation (mPFC–dPAG::ChR2/eYFP = bilateral 20 Hz 5 ms pulses, 12–15 mW) in a brightly lit room containing constant white noise (Marpac Dohm-DS dual speed sound conditioner). Behaviour was recorded via a video camera positioned directly above the arena

using Ethovision XT (Noldus). Photographs of the behavioural arena before (undisturbed) and after each 12-min session were obtained and marbles that were 100% buried were counted. Time spent digging was scored by two experimenters blind to conditions using ODLog (Macropod). Cage exploration time was obtained by subtracting the time spent of scored behaviours from the total session length. The time spent engaging in each behaviour was quantified by taking the average between the two experimenters. One mPFC–dPAG::ChR2 video was corrupted and was not included in analyses. In between subjects a new cage containing fresh bedding was used and marbles were cleaned with 15% isopropyl alcohol diluted in ddH₂O.

Following the conclusion of the experiments, a subset of rats were stimulated for 5 min in a dark, sound-attenuating room (473 nm, 20 Hz, 20 mW, 5 ms pulses) for c-Fos quantification to verify light-evoked activity in ChR2⁺ mPFC–dPAG neurons. Eighty min later, rats were deeply anaesthetized and transferred to the laboratory and transcardially perfused. Sample size was based on reports in related literature and were not predetermined by calculation.

In vivo epifluorescent calcium imaging. *Projection-specific subjects.* Male wild-type C57BL/6J mice (~8 weeks old; mPFC–dPAG::GCaMP6m and mPFC–NAc::GCaMP6m) or male DAT::IRES-Cre mice[46] (~8 weeks old; mPFC–dPAG::GCaMP6m + VTA^DA::ChrimsonR or mCherry) were group-housed (2–4 subjects per cage) on a 12:12 h reverse light:dark cycle (lights off at 09.00) before and 4 weeks following initial virus and microendoscope (that is, GRIN lens) implant surgery. Following baseplate adhesion, subjects were individually housed and placed on food restriction (3–6 g normal chow per day) with ad libitum access to water for 3–6 days encompassing testing. Sample sizes were based on reports in related literature and were not predetermined by calculation.

Surgeries. Subjects were prepared for in vivo epifluorescent calcium imaging[26] similarly to methods described elsewhere[47,48]. In brief, to achieve projection-specific imaging, a virus encoding Cre-dependent GCaMP6m (AAV5-CAG-FLEX-GCaMP6m) was injected into the mPFC (AP: +1.8, ML: +0.3, DV: −2.75 and −2.4 (300 nl each, bevel facing lateral)) and retrogradely travelling CAV2-Cre (Institut de Génétique Moléculaire de Montpellier, France) was injected into the dPAG (n = 6; AP: −4.2, ML: +0.5, DV: −2.4 (350 nl)) or the NAc shell (n = 5; AP: +1.0, ML: +0.75; DV: −4.5 (350 nl)). For manipulation of dopamine terminals in mPFC–dPAG::GCaMP6m + VTA^DA::ChrimsonR subjects (n = 4), DAT::IRES-Cre mice received 1 µl AAV8-hSyn-FLEX-ChrimsonR-tdT in the VTA (AP: −3.4, ML: +0.4, DV: −4.25). Control mice (mPFC–dPAG::GCaMP6m + VTA^DA::mCherry; n = 5), received 1 µl AAV5-EF1a-DIO-mCherry into the VTA using the same coordinates. After virus infusions, the mPFC craniotomy was enlarged to >1 mm in diameter and dura removed with a bent 30 gauge beveled needle, but no tissue was aspirated. A 1 mm diameter, ~4 mm length gradient refractive index lens (GRIN lens; GLP-1040, Inscopix) was held by vacuum on the tip of a blunted needle surrounded by plastic tubing for stability and was lowered stereotaxically through the craniotomy under constant saline perfusion to minimize tissue/blood desiccation. Lenses were implanted slightly posterior and lateral of the needle track for virus infusions to avoid tissue damage in the imaging plane, and were lowered to locations in the ventral PL/dorsal IL subregion of the mPFC (AP: −1.77, ML: −0.4, DV: −2.32, mm from bregma). Lens implants were secured to the skull with a thin layer of adhesive cement (C&B Metabond; Parkell), followed by black cranioplastic cement (Ortho-Jet; Lang) containing gentamicin antibiotic. Lenses were covered with the top of an eppendorf tube and cemented in place with cranioplastic cement for protection during the virus incubation period (3–4 weeks). The implant was allowed to completely dry before closure of the incision with nylon sutures.

Following virus incubation, mice were again anaesthetized with isoflurane, stereotaxically secured, and baseplates (Inscopix) were cemented around the lens to support the connection of the miniaturized microscope for in vivo, freely moving imaging. During this procedure, the protective eppendorf cap and supporting cranioplastic cement were removed using a hand drill. The exposed top of the GRIN lens was scrubbed clean with a cotton-tipped applicator soaked with 15% isopropyl alcohol diluted in ddH₂O. Next, a miniaturized microscope (single channel epifluorescence, 475-nm blue LED, Inscopix) with the baseplate attached was stereotaxically positioned over the implanted GRIN lens and adjusted in the DV axis in order to focus on visible landmarks (that is, GCaMP6m-expressing neurons and blood vessels). After the focal plane was identified, the microscope/baseplate was raised by ~50 µm, to account for cement shrinkage, and was subsequently cemented in place with pink dental cement (Stoelting). The microscope was then detached from the baseplates, a final layer of black cranioplastic cement (Ortho-Jet; Lang) was applied to prevent light leak, and the implant was covered with a protective plate (Inscopix) until imaging.

Behavioural sucrose/shock paradigm and data acquisition. Following recovery (~7 days), mice were individually housed and food restricted for 2 days and exposed to 30% sucrose solution (diluted in standard tap/cage H₂O) in the home cage. Food-deprived mice were then trained in operant chambers equipped with sucrose lickometers (Med Associates), with a modified spout that extended into the chamber from the recessed opening, for ~60 min while connected to a plas-

tic 'dummy' microscope for training and habituation. All animals readily self-administered sucrose via the lickometer after 2 days of training. On the testing day, food-deprived mice were gently restrained and connected with the miniaturized microscope (single channel epifluorescence, 475-nm blue LED, Inscopix) via the baseplate and secured with a small screw on the baseplate. Mice were allowed to recover from restraint for 10 min before the first session was initiated. Mice were exposed to two 15-min imaging sessions ('sucrose' and 'shock'), counterbalanced and separated by a 15-min intermediate epoch, during which the animal remained in the chamber, but no sucrose or footshocks were administered. During 'sucrose' sessions, food-deprived mice were allowed to self-administer sucrose for 15 min via the lickometer they had been exposed to previously. During 'shock' sessions, mice were exposed to 27 mild electric foot shocks (0.2 mA; 1 s duration; 10–60 s ISI) for 15 min. Grayscale tiff images were collected at 20 frames per second using 20–60% of the miniaturized microscope's LED transmission range (nVista HD V2, Inscopix).

Recording from mPFC–dPAG neurons while manipulating VTA^{DA} terminal activity. Following recovery, DAT::Cre mice were individually housed and food-restricted for 2 days before recording. Before the recording day, food-deprived mice were habituated to handling and the nVoke miniaturized microscope (an integrated imaging and optogenetics system, 455-nm blue GCaMP excitation LED, 590-nm amber optogenetic LED, Inscopix). Twenty-four hours before recordings, mice were habituated in their home cage to a dimly lit recording room containing constant white noise (Marpac Dohm-DS dual speed sound conditioner, Wilmington). On the recording day, mice were attached to the nVoke miniaturized microscope and habituated in their home cage for 15 min. After the 15-min habituation, a 30-min recording session, composed of 10-min OFF–ON–OFF epochs, was initiated. Grayscale images were collected at 10 frames per second using 0.094–0.266 mW mm^{-2} (estimated light power based on GRIN lens efficiency) of the miniaturized microscope's 455-nm LED transmission range (nVoke 2.1.5., Inscopix). During the ON epoch, 20 Hz, 60-pulse trains (5 ms each) of 620-nm LED light were initiated every 30 s for the duration of the 10-min epoch.

Image processing. Image processing was accomplished using Mosaic software (v.1.1.2., Inscopix). Raw videos were pre-processed by applying ×4 spatial downsampling to reduce file size and processing time, and isolated dropped frames were corrected. No temporal downsampling was applied. For sucrose/shock experiments, both recordings per animal (that is, 'sucrose' recording and 'shock' recording) were concatenated to generate a single 30-min video. Lateral movement was corrected for by using a portion of a single reference frame (typically a window surrounding a prominent blood vessel or constellation of bright neurons) as previously described[26,49]. Images were cropped to remove post-registration borders and sections in which cells were not observed. Two methods were used for ROI identification and single-cell fluorescence trace extraction in order to verify that these processes did not significantly change the pattern of results within our datasets. Both methods are described below in 'CNMF-E analyses' (with and without non-negative constraint on temporal components) and 'non-ROI analyses'. The results from the CNMF-E analyses with non-negative constraint are reported in Figs. 3, 4. The results from the CNMF-E analyses without non-negative constraint and non-ROI analyses are reported in Extended Data Figs. 6, 8.

CNMF-E analyses. After motion correction and cropping, recordings were exported as .tif z-stacks and were downsampled to 10 frames per second. We used a constrained non-negative matrix factorization algorithm optimized for microendoscopic imaging (CNMF-E)[28] to extract fluorescence traces from ROIs. ROIs were defined by manually selecting seed pixels from peak-to-noise (PNR) graphs of the field of view (FOV)[23]. Considering calcium fluctuations can exhibit negative transients, associated with a pause in firing[13,24], we also performed analyses in which we did not constrain temporal components to >0—these data are provided in the extended data figures.

Non-ROI analyses. After motion correction and cropping, recordings were converted to changes in fluorescence (F) compared to background fluorescence (F_0) according to the expression $(F - F_0)/F_0$, using the mean t-projection image of the entire movie as reference (F_0). Calcium signals arising from individual regions of interest (ROIs, that is, cells) were identified using independent and principal component analyses (PCA/ICA), as previously described[50]. Identified PCA/ICA filters were thresholded at their half-max values to define possible ROIs. ROIs were then screened for neuronal morphology and only accepted if the thresholded filters included only one contiguous region with an eccentricity of <0.85 and an area between 30–350 pixels. Accepted ROI filters were merged if their areas overlapped by more than 60% after visual confirmation. The accepted ROI filters were then reapplied to the motion-corrected videos to extract dF/F_0 traces for each ROI. In order to correct for bleaching and possible neuropil contamination of the extracted ROI trace, we correct each ROI tracing using signals from the whole field, using a multiple-step procedure: The full ROI trace and the signals from the whole field were filtered using a 30-s median filter to eliminate the influence of sharp transients or outliers. The influence of the surrounding signals on the ROI trace were quan-

tified using regression ('glmfit' in MATLAB). The resulting regression coefficient was then applied to the original, unfiltered trace to regress out the influence of the non-ROI thresholded field on the ROI trace itself. Multiple background subtraction methods were examined and a non-ROI thresholded approach was implemented because 1) this approach excludes subtraction of prominent processes (that is, dendrites and axons) observed in our dataset, and 2) the reasonable correlation coefficients obtained between individual ROIs are consistent with the range that would be expected based on electrical recordings. To acquire the non-ROI thresholded image for background subtraction, max t-projections of individual recordings were created and thresholded to separate ROIs and their processes from the rest of the FOV. Average signal from the remaining pixels was used as a proxy for the whole-field changes in fluorescence, and regressed from the signal from each ROI.

Data analysis. Individual lick bouts were characterized by lick events detected at the sucrose lickometer and events that were separated by >1 s were identified as an individual lick bout. Calcium signals for the bulk FOV fluorescence and for each ROI were aligned to behavioural events (that is, lick bout initiation and shock). Population z-scores were calculated using the period −10 to −5 s before stimuli onset as baseline. ROIs were classified as being stimulus-excited if the average z-score 0–1 s after stimulus onset was greater than 3.

For agglomerative clustering, we first concatenated average responses of individual neurons aligned to shocks across trials (expressed as r(shocks), in z-score), and its average response aligned to licks across trials (expressed as r(licks), in z-score), such that each row in the heat map corresponds to one neuron. There were 118 neurons from the PAG and 169 neurons from the NAc in total. Agglomerative hierarchical clustering was applied using Ward's Euclidean linkage, followed by a soft normalization: for each neuron, if its maximum absolute z-score was above 1, its z-score at each frame was divided by its maximum z-score across time. If its maximum absolute z-score was below 1, it remained unchanged. Pairs of neurons that were in close proximity were linked. As they were paired into binary clusters, the newly formed clusters were grouped into larger clusters until a hierarchical tree was formed. A threshold at 0.3× max(linkage) was set to prune branches off the bottom of the hierarchical tree, and assign all the neurons below each cut to a single cluster. After clusters were constructed, data from the PAG and the NAc separated to generate their individual heat maps using their original average response profiles (without normalization). For both areas, clusters were sorted in an ascending order on the basis of their third quartile of the response to the shocks. Within each cluster, neurons were also sorted in an ascending order on the basis of their response to the shocks. Different bars on the left side of the heat maps correspond to different clusters. The same colour suggests that they belong to the same cluster from the dendrogram. Calcium event quantifications (number and amplitude) were performed in MiniAnalysis (Synaptosoft) using individual ROI traces from the entire session after conversion to z-score. Baseline from the z transform was computed by thresholding the signal at 20% of the signal amplitude. Calcium events with z-scores <5 or those that did not have a >0.5 AUC were not included in analyses because events of this magnitude were not reliably retain transient, calcium-event characteristics across animals. ROIs that did not contain events meeting event criteria were excluded.

Ex vivo electrophysiology to examine dopamine effects on projector populations. *Subjects.* Male and female heterozygous BAC transgenic TH::Cre rats (~220 g; Charles River Laboratories) were dual-housed on a normal 12:12 h light:dark cycle (lights on at 09:00) throughout the duration of experiments. Sample sizes were based on reports in related literature and were not predetermined by calculation.

Surgery. Rats first received bilateral infusions of AAV_5-EF1a-DIO-ChR2-eYFP, as previously described (see 'FSCV Surgery'). Rats were allowed to recover for virus surgery for an 8–10 week incubation period to ensure Cre-specific viral transduction of ChR2 in VTA^{DA} neurons and protein transport to distal terminals in the mPFC. After incubation, rats received a second surgery to retrogradely label dPAG and NAc shell projectors in the mPFC. CTB injections were performed similarly as previously described ('Retrograde cholera toxin-B tracing'). In brief, rats received bilateral injections of CTB conjugated to Alexa Fluor 488 or 555 (Molecular Probes) into the dPAG (AP: −6.6, ML: −0.6; DV: −5.4 mm), the NAc (AP: +1.5, ML: +0.95, DV: −7.5 mm), or one in each hemisphere (fluorophores were counterbalanced between rats).

Brain slice preparation. Seven days following CTB injections, TH::Cre rats were deeply anaesthetized with sodium pentobarbital (250 mg kg^{-1}; intraperitoneal) and transcardially perfused with 60 ml ice-cold modified artificial cerebrospinal fluid (aCSF) (NaCl 87, KCl 2.5, NaH$_2$PO$_4$·H$_2$O 1.3, MgCl$_2$·6H$_2$O 7, NaHCO$_3$ 25, sucrose 75, ascorbate 5, CaCl$_2$·2H$_2$O 0.5 (composition in mM) in ddH$_2$O; osmolarity 322–326 mOsm, pH 7.20–7.30) saturated with carbogen gas (95% oxygen, 5% carbon dioxide). Following decapitation, the brain was rapidly removed from the cranial cavity and coronally dissected (AP: ~−1.5 mm from bregma). Coronal 300-μm brain sections were prepared from the anterior portion of the brain containing the mPFC and striatum, using a vibrating microtome (Leica VT1000S,

Leica Microsystems). The posterior portion of the brain was transferred to 4% paraformaldehyde (PFA) dissolved in $1\times$ PBS for fixation and subsequent histological processing (see below in 'Histology'). Brain slices were given at least 1 h to recover in a holding chamber containing aCSF (NaCl 126, KCl 2.5, NaH$_2$PO$_4$·H$_2$O 1.25, MgCl$_2$·6H$_2$O 1, NaHCO$_3$ 26, glucose 10, CaCl$_2$·H$_2$O 2.4 (composition in mM); in ddH$_2$O; osmolarity 298–301 mOsm; pH 7.28–7.32) saturated with carbogen gas at 32 °C before being transferred to the recording chamber for electrophysiological recordings.

Whole-cell patch-clamp recordings. Once in the recording chamber, brain slices were continually perfused with fully oxygenated aCSF at a rate of 2 ml min^{-1} at 30–32 °C. Neurons were visualized using an upright microscope (Scientifica) equipped with IR-DIC optics and a QImaging Retiga EXi camera (QImaging) through a $40\times$ water-immersion objective. Brief illumination through a 470-nm or 595-nm LED light source (pE-100; CoolLED) was used to identify CTB-488 and CTB-555-expressing mPFC neurons, respectively, before recording. Whole-cell patch-clamp recordings were performed using glass electrodes (resistance 4–6 MΩ) pulled from thin-walled borosilicate glass capillary tubing (World Precision Instruments) on a P-97 horizontal puller (Sutter Instrument) and filled with internal solution containing (in mM) potassium gluconate 125, NaCl 10, HEPES 20, Mg-ATP 3, neurobiotin 0.1% in ddH$_2$O (osmolarity 287, pH 7.33). For electrophysiological recordings, signals were amplified using a Multiclamp 700B amplifier (Molecular Devices), digitized at 10 kHz using a Digidata 1550 (Molecular Devices), and recorded using Clampex 10.4 software (Molecular Devices). Capacitance, series resistance (R_s) and input resistance (R_{in}) were frequently measured during recordings to monitor cell health, using a 5-mV hyperpolarizing step-in voltage clamp. The resting membrane potential and the current–voltage (I–V) relationship of the neuron were determined in current-clamp mode using incremental 20 pA, 500-ms square current pulses from -120 pA to $+260$ pA. The instantaneous and steady-state action potential firing frequencies were calculated using the first 100 ms and last 300 ms of the current pulse, respectively.

In order to assess the effect of activating ChR2-expressing VTA (dopamine) terminals on mPFC neuron firing, a square current pulse (2-s duration) was applied in current-clamp mode to elicit stable firing ($\sim$2–6 Hz). After 20 s a 20-Hz train of 470-nm light (5-ms pulse duration) was delivered through the $40\times$ objective for 3 s. During the last 2 s of this blue-light train, the same square current pulse was applied to the cell. This protocol was repeated every 50 s and the firing during the current pulses (with and without blue light stimulation) was used for analysis. To determine the effect of VTA (dopamine) terminal stimulation on the rheobase of the neuron, the same protocol was performed, but instead of a square current pulse, a 2-s current ramp was applied to the cell.

The D2-type dopamine-receptor antagonist raclopride was used in a subset of recordings during which a square current pulse was applied with and without optical stimulation of ChR2-expressing VTA (dopamine) terminals. Raclopride (Sigma-Aldrich) was prepared fresh at the start of each recording session and was dissolved in aCSF to give a final concentration of 10 μM. Raclopride was perfused onto the slice for at least 10 min before electrophysiological recordings were commenced.

Analysis of action potential firing was performed offline using Clampfit 10.4 software (Molecular Devices) and passive membrane properties were computed using custom MATLAB software written by P.N. based on MATLAB implementation of the Q method[51].

Immunohistochemistry. Following recording, slices were transferred to 4% PFA solution overnight at 4 °C, and were then washed four times (for 10 min each) in $1\times$ PBS. Slices were then blocked in $1\times$ PBS solution containing 0.3% Triton X-100 and 5% normal donkey serum (NDS; Jackson ImmunoResearch) for 1 h at room temperature. They were then incubated in primary antibody solution containing chicken anti-TH antibody (1:1,000; Millipore, MA, USA) in $1\times$ PBS with 0.3% Triton X-100 (Thermo Fisher Scientific) and 3% NDS overnight at 4 °C. Slices were subsequently washed four times (for 10 min each) in $1\times$ PBS and then incubated in secondary antibody solution containing Alexa Fluor 647-conjugated donkey anti-chicken (1:1,000; Jackson ImmunoResearch) and Alexa Fluor 405-conjugated streptavidin (1:1,000; Biotium) in $1\times$ PBS with 0.1% Triton X-100 and 3% NDS for 2 h at room temperature. Slices were finally washed five times (for 10 min each) in $1\times$ PBS, then mounted onto glass slides and coverslipped using polyvinyl alcohol (PVA) mounting medium with DABCO (Sigma-Aldrich).

Ex vivo electrophysiology to determine latency for phototagging experiments.
Subjects and surgery. To verify the latency of blue-light-evoked action potentials in ChR2-expressing mPFC–dPAG projectors, DAT::Cre mice were used, which had received the same viral surgery as those for in vivo electrophysiology experiments. Viral incubation for ex vivo recordings was matched for those for in vivo experiments. For subject and surgery details, see below, 'In vivo electrophysiology, surgery'.
Brain slice preparation. Brian slice preparation was similar to the previously described method in 'ex vivo electrophysiology to examine dopamine effects on projector populations'. In brief, mice were deeply anaesthetized with sodium

pentobarbital (90 mg kg^{-1}; intraperitoneal) and transcardially perfused with 20 ml ice-cold modified aCSF (NaCl 87, KCl 2.5, NaH$_2$PO$_4$·H$_2$O 1.3, MgCl$_2$·6H$_2$O 7, NaHCO$_3$ 25, sucrose 75, ascorbate 5, CaCl$_2$·2H$_2$O 0.5 (composition in mM) in ddH$_2$O; osmolarity 322–326 mOsm, pH 7.20–7.30) saturated with carbogen gas (95% oxygen, 5% carbon dioxide). Following decapitation, the brain was rapidly removed from the cranial cavity and coronally dissected (AP: $\sim$0 mm from bregma). Coronal 300-μm brain sections were prepared from the anterior portion of the brain containing the mPFC and striatum, using a vibrating microtome (Leica VT1000S, Leica Microsystems). The posterior portion of the brain was transferred to 4% PFA dissolved in $1\times$ PBS for fixation and subsequent histological processing (see below in 'Histology'). Brain slices were given at least 1 h to recover in a holding chamber containing aCSF (NaCl 126, KCl 2.5, NaH$_2$PO$_4$·H$_2$O 1.25, MgCl$_2$·6H$_2$O 1, NaHCO$_3$ 26, glucose 10, CaCl$_2$·H$_2$O 2.4 (composition in mM); in ddH$_2$O; osmolarity 298–301 mOsm; pH 7.28–7.32) saturated with carbogen gas at 32 °C before being transferred to the recording chamber for electrophysiological recordings.

Whole-cell patch-clamp recordings. Recordings were similar to those previously described above. In brief, recordings were made from visually identified neurons expressing ChR2–eYFP and non-expressing neighbours. Blue light was provided by a 470-nm LED light source (pE-100; CoolLED) delivered through a $40\times$ immersion objective. ChR2 expression in recorded neurons was confirmed by the presence of sustained inward current in response to 1-s constant pulse of blue light delivered in voltage-clamp mode.

Offline analysis was performed in Clampfit 10.4 software (Molecular Devices). Latency to action potential or excitatory postsynaptic potential (EPSP) peak were averaged from 30 responses to a 5-ms pulse of blue light (delivered in a 10-pulse, 1-Hz train every 60 s). Latency was measured as the duration from the onset of the light pulse to the peak of the action potential or EPSP.

Dopamine receptor localization on projector populations. *Subjects.* Transgenic male and female Drd1a-Cre ($n = 3$, B6.FVB(Cg)-Tg(Drd1a-cre)FK150Gsat/ Mmucd ; ID# 036916-UCD from MMRRC originally from GENSAT BAC Tg project) and Drd2-Cre mice ($n = 3$, B6.FVB(Cg)-Tg(Drd2-cre)ER44Gsat/Mmucd ; ID# 032108-UCD from MMRRC originally from GENSAT BAC Tg project) ($\sim$12 weeks old) were group-housed (2–4 subjects per cage) on a 12:12 h reverse light:dark cycle (lights off at 09.00) throughout the duration of experiments with ad libitum access to food and water. Sample sizes were based on reports in related literature and were not predetermined by calculation.

Surgeries. To label Drd1a- and Drd2-expressing mPFC neurons, AAV$_5$-EF1a-DIO-eYFP was injected bilaterally into the mPFC (AP: $+1.8$, ML: $+0.3$, DV: -2.75 and -2.4 (300 nl each, bevel facing lateral). Mice were allowed to recover and incubate for 4 weeks. In a second surgery, 350 nl CTB conjugated to Alexa Fluor 555, or 647 (Molecular Probes) was injected into the dPAG (AP: -4.2, ML: -0.5; DV: -2.4 mm) and NAc shell (AP: $+1.0$, ML: $+0.75$, DV: -4.5 mm) (in contralateral hemispheres, colour counterbalanced) to retrogradely label mPFC–dPAG and mPFC–NAc projectors. Mice were euthanized 6 days later as previously described. Histological, imaging, and data analyses are similar to those described above.

In vivo electrophysiology. *Subjects.* Male DAT::IRES-Cre mice ($\sim$6–8 weeks old) were group-housed (2–4 subjects per cage) on a 12:12 h reverse light:dark cycle (lights off at 09.00) throughout the duration of experiments. Two days after head-bar adhesion ($\sim$2 weeks before recordings), cages were placed on food restriction (4 h access to standard chow per day) with ad libitum access to water throughout training and recording. Sample sizes were based on reports in related literature and were not predetermined by calculation.

Surgery. To achieve projection-specific ChR2 expression for in vivo photoidentification of mPFC–dPAG projectors, a virus encoding Cre-dependent ChR2 (AAV$_5$-EF1a-DIO-ChR2-eYFP) was injected into the mPFC (AP: $+1.8$, ML: $+0.3$, DV: -2.75 and -2.4 (300 nl each, bevel facing lateral)) and retrogradely travelling CAV2-Cre (Institut de Génétique Moléculaire de Montpellier, France) was injected into the dPAG (AP: -4.2, ML: $+0.5$, DV: -2.4 (350 nl)). For manipulation of dopamine terminals, DAT::IRES-Cre mice received 1 μl AAV$_8$-hSyn-FLEX-ChrimsonR-tdT in the VTA (AP: -3.4, ML: $+0.4$, DV: -4.25).

Head-bar adhesion. After 11+ weeks of virus incubation, and $\sim$2 weeks before behavioural training, mice were briefly anaesthetized and a small aluminium head-bar (2 cm $\times$ 2 mm $\times$ 2 mm) was placed on the skull 5 mm posterior to the bregma along with one reference and one ground pin contacting the dura mater just anterior to the head-bar, in the contralateral cortex. A small pilot hole was made with a cranial drill above the mPFC and was marked with a pen. The area surrounding the pilot hole/mark was covered with petroleum jelly to prevent covering with dental cement. The three elements (head-bar, ground pin and reference pin) were cemented using one layer of adhesive cement (C&B metabond; Parkell) followed by a layer of cranioplastic cement (Dental cement; Stoelting). After the cement dried, the pilot hole/mark was covered with a silicone gel (Kwik-Sil Adhesive, WPI) to keep the bone clear during behavioural training.

Behaviour. Two days after head-bar adhesion, mice were food restricted and pre-exposed to a 30% sucrose solution. Mice were head-fixed[30] in front of two

small tubes, one located just under the nose and the other above it pointed at the nose. The bottom tube delivered sucrose (training and recording days) and the top tube delivered airpuff (recording days only). Mice were trained to retrieve small drops (3 µl) of sucrose delivered through the bottom tube via a solenoid valve (Parker), measured by breaks of an infrared beam recorded by an Arduino board (SmartProjects). Training sessions gradually increased in total duration (0.5–1.5 h) and sucrose ITIs increased (15–80 ± 8 s) over 5–8 days. The solenoid valves were triggered with a custom software written in LabVIEW (National Instruments) powered by NIDAQ-6251 and Arduino hardware.

Pre-recording craniotomy. After 5–8 days of habituation and training, mice were briefly anaesthetized with isoflurane (5% for induction, 1.5% after) and placed in a stereotaxic frame while their body temperature was controlled with a heating pad. A craniotomy was performed over the mPFC using the pilot hole/mark previously implemented using a hand-held drill. When the craniotomy was open, the dura was removed, blood cleaned with perfusion of saline, and then covered with petroleum jelly. Mice were removed from the stereotaxic frame and placed in a clean cage while their body temperature was maintained using a heat lamp until they fully recovered from anaesthesia.

In vivo electrophysiological recordings and phototagging. Once the mice recovered from the craniotomy surgery (at least 1 h), they were head-fixed and a silicon optrode (A1x16-Poly2-5mm-50 s- 177, NeuroNexus) coated with red fluorescent latex microspheres (Lumafluor) was inserted into the anterior mPFC and lowered from the surface of the cortex for 1 mm at 10 µm s^{-1} using a motorized actuator (Z825B - 25 mm Motorized Actuator, Thorlabs) mounted on a shuttle (460A linear stage, Newport) fixed to the stereotaxic arm. Next, the optrode was lowered for 1 mm at 1–2 µm s^{-1}. During the insertion of the electrode, sucrose was delivered every 60 ± 8 s. After the probe was lowered to −2 mm below brain surface, sucrose deliveries were halted and a 10-min wait period commenced to let the tissue stabilize around the recording probe. Recording sessions were initiated using a RZ5D TDT system (Tucker-Davis Technologies) while presenting ~40 sucrose and 40 airpuff trials (11 ± 5 s ITI) randomly intermixed throughout the entire 30-min recording period. The recording period was broken into three 10-min epochs: 10 min into the recording period (first OFF epoch), 593-nm laser-light pulse trains (20 Hz, 60 pulses of 5 ms) were delivered through the optrode every 30 s for 10 min (20 pulse trains total, ON epoch). Ten more minutes were recorded in the absence of laser manipulation (second OFF epoch)—resulting in an OFF–ON–OFF epoch structure, with laser delivery occurring only during the ON epoch. Following completion of a 30-min recording session, a photoidentification session using a 473 and/or 405-nm laser was conducted, during which pseudorandomly dispersed stimulations were delivered: 1-s constant light, 10× 1 Hz, 5-ms pulse trains, and 100 ms of 100 Hz (5-ms pulses). Recordings were then terminated and the optrode was lowered 300 µm to a new recording site at 1–2 µm s^{-1}. The recording protocol was then repeated after a 30-min inter-session interval. Recordings sessions continued until we reached the bottom of the mPFC (−3 mm from brain surface) or when mice became sated and stopped retrieving sucrose. The electrode was then retracted at 5 µm s^{-1}, the craniotomy cleaned with saline, and covered with silicone gel (Kwik-Sil Adhesive, WPI) to protect the brain until the next day of recording. During the second day of recording, the same procedure was repeated in a more posterior recording location. Following completion of the second day of recordings, mice were anaesthetized with sodium pentobarbital and transcardially perfused. The brain was extracted, sectioned, and examined under a confocal microscope to verify the viral expression and the locations of the recording electrode.

Analysis of in vivo electrophysiological recordings. Recording sessions were exported from the TDT format to Plexon offline sorter using OpenBridge (Tucker-Davis Technologies). Offline sorter (Plexon) was used to sort single units. Neural responses to sucrose/airpuff delivery and light stimulation were visualized through peristimulus time histograms (PSTH) and rasters for every unit using NeuroExplorer.

Data from Plexon and Neuroexplorer data files were then imported into MATLAB and analysed using software written by P.N. Sucrose and airpuff PSTHs for each epoch (OFF–ON–OFF) were z-transformed using the histogram values in a 2-s baseline period starting 3 s before the onset of the stimulus. Similarly, PSTHs around a light pulse (used for photoidentification of dPAG projectors) were z-transformed using a baseline window of 40 ms before the onset of the light pulse. To test the significance of neural responses, Wilcoxon signed-rank tests were performed on the neural activity of each unit by comparing the number of spikes in a baseline window and an experimental window starting at the onset of stimulus or light pulse. The experimental window for AUC stimulus response was set to 0.5 s. The experimental window for light response was 8 ms based on the results of ex vivo recordings. The significance threshold for the Wilcoxon signed-rank test was set at $P < 0.01$. Latency to the light pulse was defined as the first bin in the PSTH to cross 4 standard deviations relative to the 40-ms baseline window. Only units which met both criteria were considered phototagged and thus mPFC–dPAG projectors. Burst analyses were performed in NeuroExplorer using interval

specifications. Bursts defined as three or more consecutive spikes with an interval of less than 25 ms in between the first two spikes and less than 50 ms in subsequent spikes, as previously defined for the mPFC[52].

Histology. *Perfusion and storage.* Subjects were deeply anaesthetized with sodium pentobarbital (200 mg kg^{-1}; intraperitoneal injection) and transcardially perfused with 15 ml (mouse) or 60 ml (rat) of Ringer's solution followed by 15 ml (mouse) or 60 ml (rat) of cold 4% PFA dissolved in 1× PBS. Animals were decapitated and the brain was extracted from the cranial cavity and placed in 4% PFA solution and stored at 4 °C for at least 48 h. Thirty-six hours before tissue sectioning, brains were transferred to 30% sucrose solution dissolved in 1× PBS at room temperature. Upon sinking, brains were sectioned at 60 µm on a freezing sliding microtome (HM420; Thermo Fisher Scientific). Sections were stored in 1× PBS at 4 °C until immunohistochemical processing.

Immunohistochemistry. Sections were blocked in 1× PBS with 0.3% Triton containing 3% NDS (Jackson ImmunoResearch), for 1 h at room temperature followed by incubation in primary antibody solution: chicken anti-TH (1:1,000; Millipore) or rabbit anti c-Fos (1:500; Santa Cruz Biotechnology) in 1× PBS with 0.1% Triton containing 3% NDS for 48 h at 4 °C. Sections were then washed 4 times (10 min each) with 1× PBS and immediately transferred to secondary antibody solution: AlexaFluor 647-conjugated donkey anti-chicken (1:1,000; Jackson ImmunoResearch) or Cy3 donkey anti-rabbit (1:500, Jackson ImmunoResearch) and a DNA-specific fluorescent probe (DAPI; 1:50,000) in 1× PBS containing 3% NDS for 2 h at room temperature. Sections not processed for immunohistochemistry were incubated in 1× PBS with 0.3% Triton containing 3% NDS and DAPI (1:50,000) for 1 h. Sections were washed 4 times (10 min each) in 1× PBS and mounted onto glass slides. Slices were allowed to dry and were coverslipped using PVA mounting medium with DABCO (Sigma). Stereotaxic coordinates were determined using brain atlases for rat[53] and mouse[54].

Confocal microscopy. Fluorescent images were captured using a confocal laser scanning microscope (Olympus FV1000), with FluoView software (Olympus), under a dry 10× / 0.40-NA objective, a 60×/1.42-NA oil-immersion objective, or a 40× /1.30-NA oil-immersion objective. The locations of opsin expression, injection site, lesion from the optic fibre placement, and the position of carbon-fibre recording electrodes were determined by taking serial z-stack images through the 10× objective across a depth of 20–40 µm, with an optical slice thickness of 5–8 µm. High-magnification images for fluorescence quantifications were obtained through the 40× or 60× objective using serial z-stack images with an optical slice thickness of 3–4 µm (5 slices) using matched parameters and imaging locations. Fluorescence (in arbitrary units) was obtained from analysis using Fiji. For quantitation of fluorescence across layers in the mPFC, measurements were normalized to the z stack containing the maximum value.

Sholl analysis. Neurobiotin-filled, streptavidin-stained mPFC–dPAG and mPFC–NAc projectors from ex vivo electrophysiology experiments were imaged at 40× (1.30-NA oil-immersion objective) using a confocal laser-scanning microscope (Olympus FV100) covering the whole dendritic and axonal arborization in the slice. Neurons were reconstructed and Sholl analysis (number of intersections, 20-µm rings from soma) performed using the 'simple neurite tracer' plugin in Fiji (http://snyderlab.com/2016/05/25/tracing-neurons-using-fiji-imagej/).

Statistics. Statistical analyses were performed using GraphPad Prism (GraphPad Software) and MATLAB (MathWorks). Group comparisons were made using one-way or two-way ANOVA followed by Bonferroni post-hoc tests to control for multiple comparisons. Paired and unpaired two-way Student's t-tests were used to make single-variable comparisons. Unpaired one-way t-tests were used to make comparisons with a priori hypotheses (time spent digging in marble burying assay). Tests for binomial distribution were also used on single populations. Non-parametric Wilcoxon signed-rank tests were used to make comparisons between non-parametric data. χ^2 tests were used to compare distribution of responsive cells between mPFC–dPAG and mPFC–NAc. All statistical tests were two-tailed unless otherwise noted as an a priori hypothesis. Thresholds for significance were placed at $*P < 0.05$, $**P < 0.01$ and $***P < 0.001$. All data are shown as mean ± s.e.m.

Reporting summary. Further information on research design is available in the Nature Research Reporting Summary linked to this paper.

Data availability

Data, unprocessed and unpseudocoloured images, and custom MATLAB codes are available upon request.

31. Nagel, G. et al. Channelrhodopsin-2, a directly light-gated cation-selective membrane channel. *Proc. Natl Acad. Sci. USA* **100**, 13940–13945 (2003).
32. Zhang, F., Wang, L.-P., Boyden, E. S. & Deisseroth, K. Channelrhodopsin-2 and optical control of excitable cells. *Nat. Methods* **3**, 785–792 (2006).
33. Gradinaru, V., Thompson, K. R. & Deisseroth, K. eNpHR: a *Natronomonas* halorhodopsin enhanced for optogenetic applications. *Brain Cell Biol.* **36**, 129–139 (2008).

34. Schobert, B. & Lanyi, J. K. Halorhodopsin is a light-driven chloride pump. *J. Biol. Chem.* **257**, 10306–10313 (1982).
35. Akerboom, J. et al. Genetically encoded calcium indicators for multi-color neural activity imaging and combination with optogenetics. *Front. Mol. Neurosci.* **6**, 2 (2013).
36. Kremer, E. J., Boutin, S., Chillon, M. & Danos, O. Canine adenovirus vectors: an alternative for adenovirus-mediated gene transfer. *J. Virol.* **74**, 505–512 (2000).
37. Schindelin, J., Arganda-Carreras, I., & Frise, E. Fiji: an open-source platform for biological-image analysis. *Nat. Methods* **9**, 676–682 (2012).
38. Witten, I. B. et al. Recombinase-driver rat lines: tools, techniques, and optogenetic application to dopamine-mediated reinforcement. *Neuron* **72**, 721–733 (2011).
39. Tsai, H.-C. et al. Phasic firing in dopaminergic neurons is sufficient for behavioral conditioning. *Science* **324**, 1080–1084 (2009).
40. Nieh, E. H. et al. Inhibitory input from the lateral hypothalamus to the ventral tegmental area disinhibits dopamine neurons and promotes behavioral activation. *Neuron* **90**, 1286–1298 (2016).
41. Sparta, D. R. et al. Construction of implantable optical fibers for long-term optogenetic manipulation of neural circuits. *Nat. Protoc.* **7**, 12–23 (2011).
42. Robinson, D. L., Venton, B. J., Heien, M. L. A. V. & Wightman, R. M. Detecting subsecond dopamine release with fast-scan cyclic voltammetry in vivo. *Clin. Chem.* **49**, 1763–1773 (2003).
43. Keithley, R. B. & Wightman, R. M. Assessing principal component regression prediction of neurochemicals detected with fast-scan cyclic voltammetry. *ACS Chem. Neurosci.* **2**, 514–525 (2011).
44. Keithley, R. B., Heien, M. L. & Wightman, R. M. Multivariate concentration determination using principal component regression with residual analysis. *Trends Anal. Chem.* **28**, 1127–1136 (2009).
45. Conte, W. L., Kamishina, H. & Reep, R. L. Multiple neuroanatomical tract-tracing using fluorescent Alexa Fluor conjugates of cholera toxin subunit B in rats. *Nat. Protoc.* **4**, 1157–1166 (2009).
46. Zhuang, X., Masson, J., Gingrich, J. A., Rayport, S. & Hen, R. Targeted gene expression in dopamine and serotonin neurons of the mouse brain. *J. Neurosci. Methods* **143**, 27–32 (2005).
47. Resendez, S. L. et al. Visualization of cortical, subcortical and deep brain neural circuit dynamics during naturalistic mammalian behavior with head-mounted microscopes and chronically implanted lenses. *Nat. Protoc.* **11**, 566–597 (2016).
48. Jennings, J. H. et al. Visualizing hypothalamic network dynamics for appetitive and consummatory behaviors. *Cell* **160**, 516–527 (2015).
49. Ziv, Y. et al. Long-term dynamics of CA1 hippocampal place codes. *Nat. Neurosci.* **16**, 264–266 (2013).
50. Mukamel, E. A., Nimmerjahn, A. & Schnitzer, M. J. Automated analysis of cellular signals from large-scale calcium imaging data. *Neuron* **63**, 747–760 (2009).
51. Novák, P. & Zahradník, I. Q-method for high-resolution, whole-cell patch-clamp impedance measurements using square wave stimulation. *Ann. Biomed. Eng.* **34**, 1201–1212 (2006).
52. Burgos-Robles, A., Vidal-Gonzalez, I., Santini, E. & Quirk, G. J. Consolidation of fear extinction requires NMDA receptor-dependent bursting in the ventromedial prefrontal cortex. *Neuron* **53**, 871–880 (2007).
53. Paxinos, G. & Watson, C. *The Rat Brain in Stereotaxic Coordinates: Hard Cover Edition* (Academic, Cambridge, MA, 2006).
54. Paxinos, G. & Franklin, K. B. *The Mouse Brain in Stereotaxic Coordinates* (Gulf, Houston, 2004).
55. Kupferschmidt, D. A., Juczewski, K., Johnson, K. A. & Lovinger, D. M. Parallel, but dissociable, processing in discrete corticostriatal inputs encodes skill learning. *Neuron* **96**, 476–489 (2017).
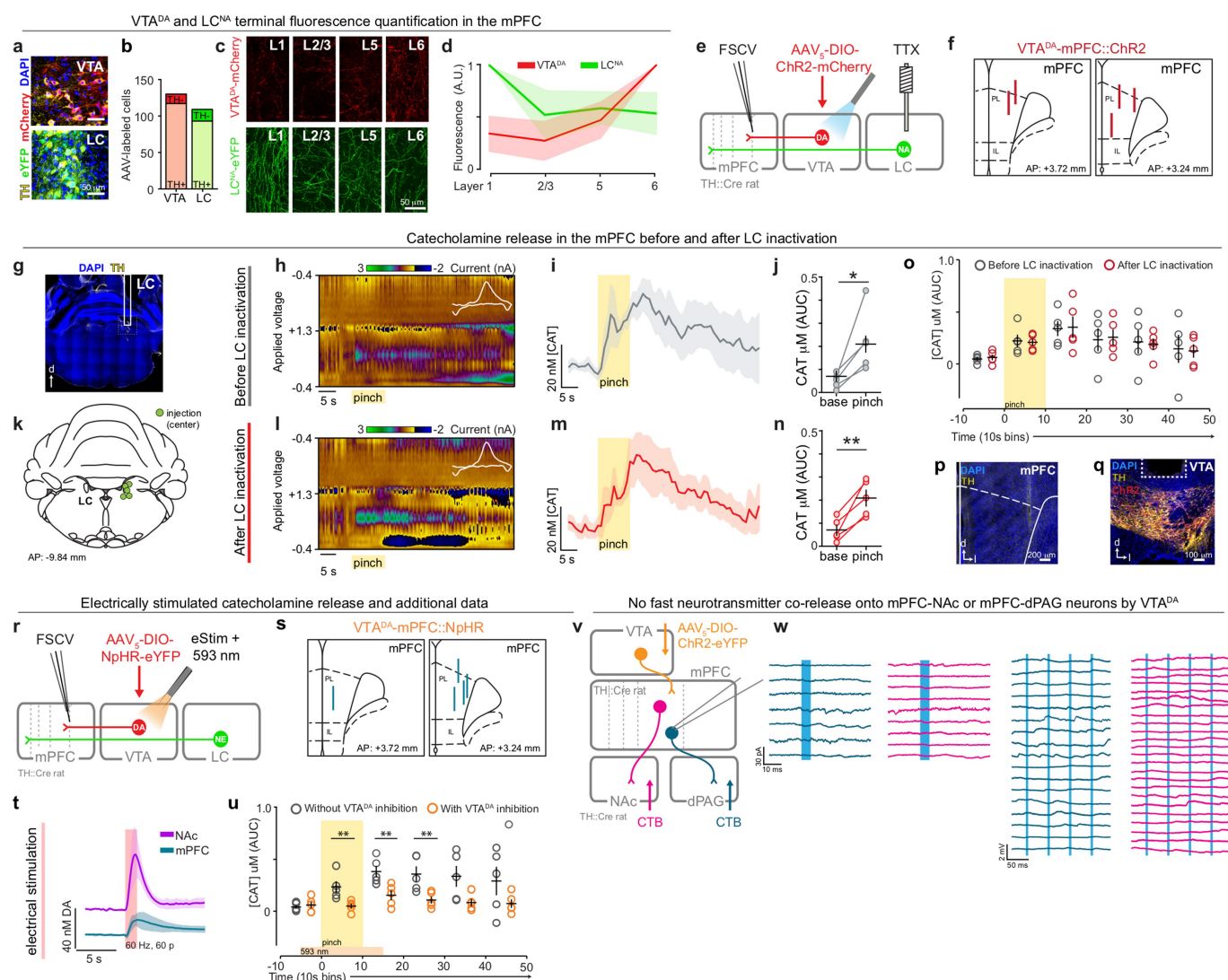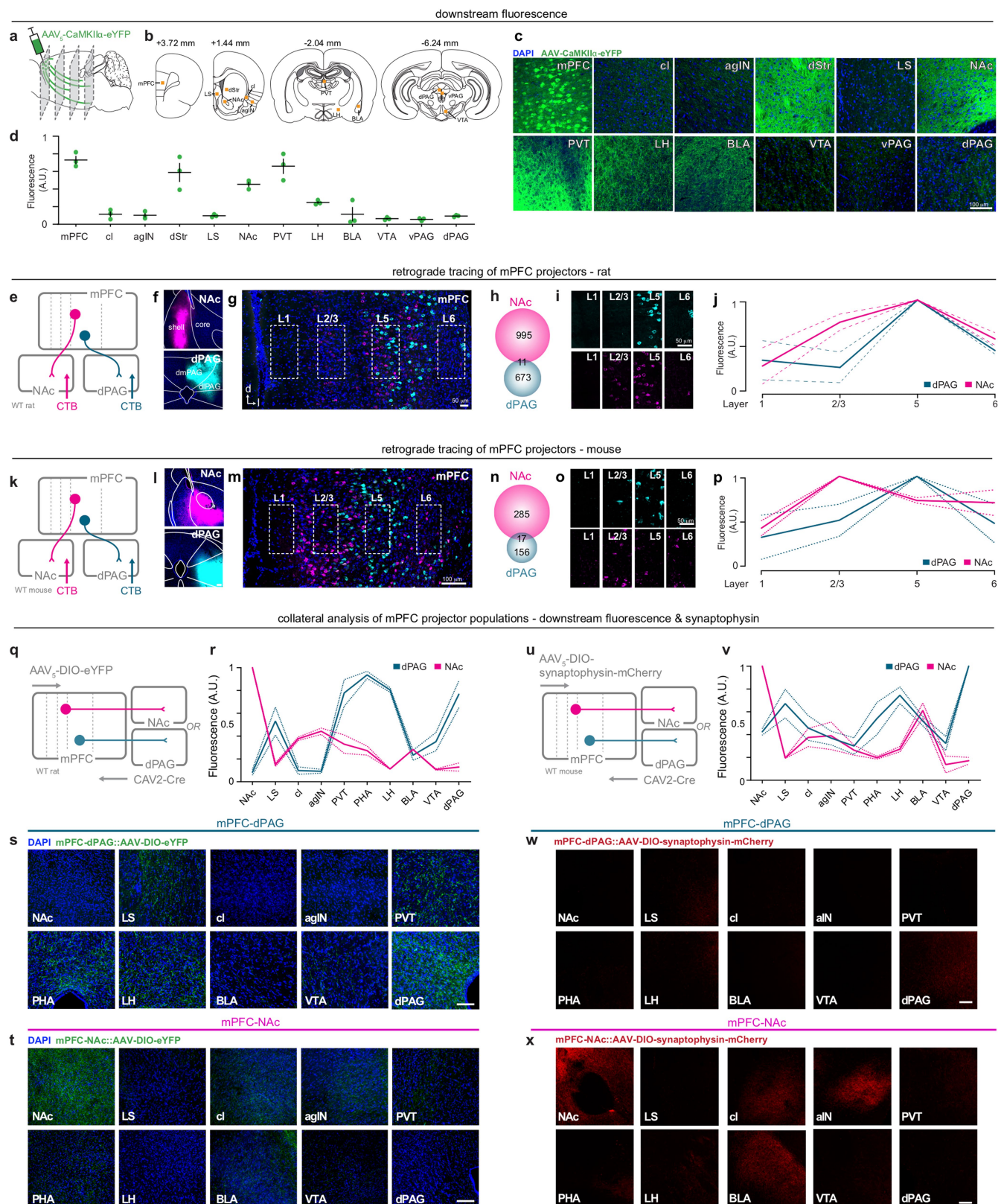
Extended Data Fig. 1 | Investigation of catecholamine terminal density and dopamine release dynamics in the mPFC. a, b, Injection of viral constructs (**a**) enabling Cre-dependent expression into the LC and VTA of TH::Cre mice resulted in (**b**) fluorescent labelling of TH positive (TH+) noradrenergic (NE) neurons in the LC and dopamine neurons in the VTA. **c,** Examination of VTA^DA and LC^NA fluorescent terminal labelling in the mPFC revealed different patterns of innervation by VTA^DA and LC^NA neurons across cortical layers in the prelimbic subregion of the mPFC ($n = 3$ mice). **d,** VTA^DA terminals were densest in the deep (5 and 6) layers of the mPFC, whereas LC^NA terminals were denser in superficial (1 and 2/3) layers. **e,** Schematic of strategy for differentiating dopamine and noradrenaline neurotransmission in the mPFC using FSCV. VTA^DA neurons were selectively transduced with ChR2 in TH::Cre rats. After incubation, rats were prepared for anaesthetized FSCV recordings, in which an optical fibre was implanted over the VTA and a guide cannula was positioned over the LC for TTX-mediated pharmacological inhibition. **f,** A glass-encased carbon-fibre recording electrode was lowered into the mPFC for FSCV neurochemical measurements. Schematic representation of all recording electrode locations for ChR2 FSCV experiments. **g,** Representative image of guide cannula track positioned over LC^NA cell bodies. Yellow, TH. **h–j,** When VTA^DA and LC^NA neurons were intact, tail pinch (10 s in duration) rapidly increased extracellular catecholamine concentration (CAT), as shown in a representative false colour plot (**h**), average CAT trace (**i**), and concentration quantification (**j**). $n = 5$ rats; two-tailed paired t-test, $t_4 = 3.402$, $*P = 0.027$. Colour plot insets, representative cyclic voltammograms. **k,** TTX–Fast Green injection

locations. **l–n,** After LC inactivation via intra-LC infusion of TTX, tail-pinch-evoked responses were maintained (two-tailed paired t-test, $t_4 = 5.249$, $**P = 0.006$. **o,** Pharmacological inactivation of the LC with TTX did not significantly alter tail-pinch-evoked catecholamine release in the mPFC. Two-way repeated measures ANOVA, $F_{5,40} = 0.061$, $P = 0.997$. **p,** Representative image of FSCV electrode track in the mPFC. **q,** Representative confocal image of ChR2–mCherry expression (red) in VTA^DA cell bodies. Yellow, TH immunostaining. **r,** Schematic of strategy to verify dependence of pinch-evoked increases in CAT neurotransmission on VTA^DA neurons. **s,** Histologically verified FSCV recording electrode locations for NpHR experiments. **t,** Electrical stimulation (60 Hz, 60 pulses, 200 µA) of the dorsal VTA evoked distinct patterns of dopamine release in the NAc and mPFC ($n = 5$ rats). **u,** Optical inhibition (20 s constant 593 nm, 5 mW) of NpHR-expressing VTA^DA neurons attenuated tail-pinch-evoked CAT release in the mPFC. Two-way repeated measures ANOVA, $F_{5,40} = 2.857$, $P = 0.027$; Bonferroni post-hoc tests, $**P < 0.01$. **v,** Schematic of viral strategy to optically manipulate ChR2-expressing VTA^DA terminals in the mPFC and record from dPAG- and NAc-projectors retrogradely labelled with CTB with ex vivo electrophysiology. **w,** No evidence of co-release of fast-synaptic neurotransmitters (that is, glutamate and GABA (γ-aminobutyric acid)) from VTA^DA terminals onto either mPFC–dPAG (teal) or mPFC–NAc (pink) populations following optical stimulation in voltage-clamp (left) and current-clamp (right). Error bars and shading represent s.e.m. A.U., arbitrary fluorescence units. The rat brain in this figure was reproduced with permission from Paxinos and Watson, 2006[53].
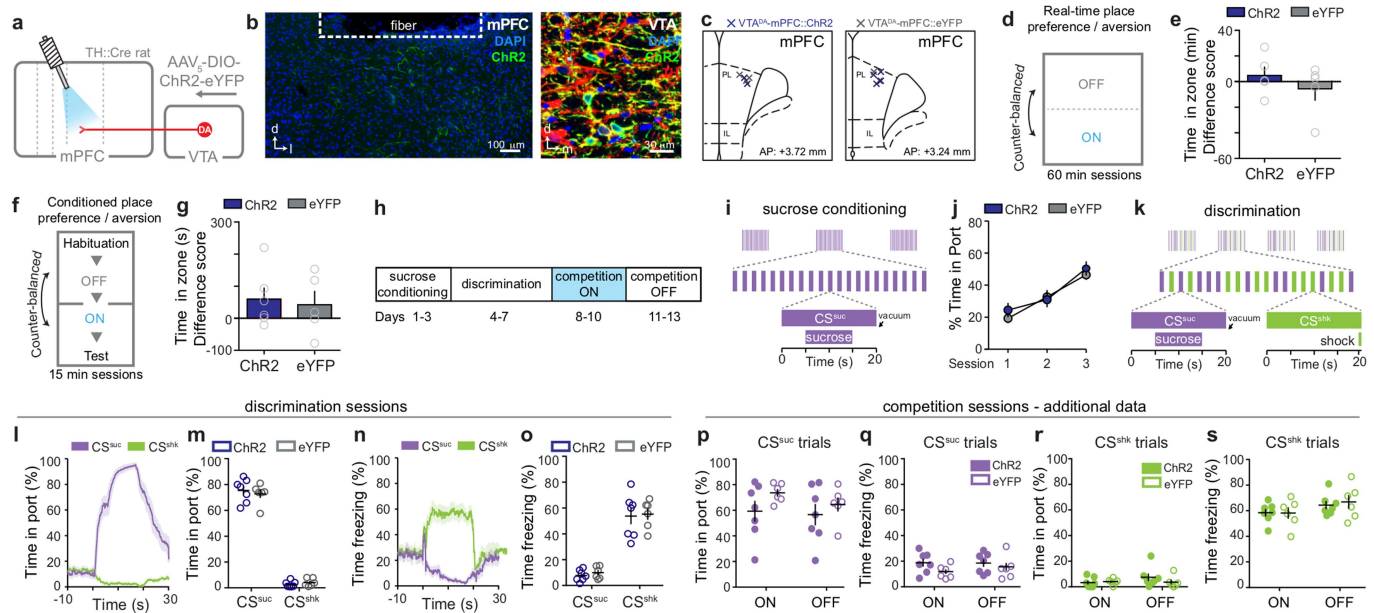
Extended Data Fig. 2 | Activation of VTA^{DA} terminals in the mPFC does not support real-time or conditioned place preference. a, Schematic of strategy for manipulating dopamine release in the mPFC. VTA^{DA} neurons were selectively transduced with ChR2 in TH::Cre rats and guide cannulae were implanted over the mPFC for the insertion of an optical fibre for light delivery. **b**, Representative confocal image of ChR2–eYFP expression in VTA^{DA}–mPFC underneath a guide cannula (left) and expression in the VTA (right). **c**, Histological verification of guide cannulae placements in the mPFC for ChR2 subjects (left) and eYFP controls (right). **d**, Schematic of experimental design for RTPP/A. When rats entered the ON zone, laser light stimulation was activated for the duration of the time spent in the ON zone (20 Hz, 60 pulses, every 30 s, 20 mW of 473 nm). When rats entered the OFF zone, light stimulation was terminated for the duration of time spent in the OFF zone. **e**, Optogenetic stimulation of VTA^{DA} terminals did not evoke real-time place avoidance or preference in VTA^{DA}–mPFC::ChR2 rats ($n = 5$), compared to VTA^{DA}–mPFC::eYFP controls ($n = 5$), measured by difference score (minutes spent in the ON zone − minutes spent in the OFF zone). Two-tailed unpaired t-test, $t_8 = 0.9337$, $P = 0.3778$. **f**, Schematic of experimental design for CPP/A. Day 1 consisted of a habituation period in which time spent on each compartment of the arena was recorded. On days 2 and 3, a divider was placed in the middle of the chamber to separate the two compartments and rats received either no stimulation (OFF) or stimulation (ON) (20 Hz, 60 pulses, every 30 s, 20 mW), counterbalanced across days. On day 4, the divider was removed and time spent in each compartment was recorded in the absence of stimulation (that is, test day). **g**, Optogenetic stimulation of VTA^{DA} terminals did not support conditioned place aversion or preference in VTA^{DA}–mPFC::ChR2 animals ($n = 6$), compared to VTA^{DA}–mPFC::eYFP controls ($n = 5$), measured by difference score. Two-tailed unpaired t-test, $t_9 = 0.3192$, $P = 0.7569$. **h**, Schematic of task used to examine dopamine modulation of reward and fear-motivated behaviours during competition. **i**, During sucrose training, a conditioned stimulus (CS) (light or tone, counterbalanced) predicted sucrose delivery (CS^{suc}).

Sucrose was removed from the delivery port by vacuum if not collected. **j**, VTA^{DA}–mPFC::ChR2 rats ($n = 7$) and VTA^{DA}–mPFC::eYFP controls ($n = 6$) acquired sucrose conditioning similarly. Two-way repeated measures ANOVA, $F_{2,22} = 0.7$, $P = 0.5090$. **k**, During discrimination, the alternative CS (light or tone, counterbalanced) was introduced and predicted foot shock (CS^{shk}). **l**, Average traces showing time spent in the sucrose port before, during, and after each CS presentation (grouped, $n = 13$ rats). **m**, Time spent in the sucrose port did not differ between VTA^{DA}–mPFC::ChR2 rats ($n = 7$) and VTA^{DA}–mPFC::eYFP controls ($n = 6$) during CS^{suc} or CS^{shk} presentation. Repeated measures two-way ANOVA, $F_{1,11} = 0.54$, $P = 0.4789$. **n**, Average traces showing time spent freezing before, during, and after each CS presentation (grouped, $n = 13$ rats). **o**, Time spent freezing did not differ between VTA^{DA}–mPFC::ChR2 rats and VTA^{DA}–mPFC::eYFP controls during CS^{suc} or CS^{shk} presentation. Repeated measures two-way ANOVA, $F_{1,11} = 0.01$, $P = 0.9281$. **p**, During competition sessions, the average time spent in the reward port for CS^{suc} trials during ON sessions and CS^{suc} trials during OFF sessions did not differ between ChR2 rats ($n = 7$, closed) and eYFP controls ($n = 6$, open). Repeated measures two-way ANOVA, $F_{1,11} = 0.82$, $P = 0.3845$. Note that during ON sessions, stimulation was only delivered during the CS^{comp} trials. **q**, Average time spent freezing for CS^{suc} trials during ON sessions and CS^{suc} trials during OFF sessions did not differ between ChR2 rats (closed) and eYFP controls (open). Repeated measures two-way ANOVA, $F_{1,11} = 1.35$, $P = 0.2705$. **r**, During competition sessions, the average time spent in the reward port for CS^{shk} trials during ON sessions and CS^{shk} trials during OFF sessions was not different between ChR2 (closed) and eYFP controls (open). Repeated measures two-way ANOVA, $F_{1,11} = 0.94$, $P = 0.354$. **s**, During competition sessions, the average time spent freezing for CS^{shk} trials during ON sessions and CS^{shk} trials during OFF sessions was not different between ChR2 rats (closed) and eYFP controls (open). Repeated measures two-way ANOVA, $F_{1,11} = 0.16$, $P = 0.6998$. Error bars and shading represent s.e.m.

downstream fluorescence

retrograde tracing of mPFC projectors - rat

retrograde tracing of mPFC projectors - mouse

collateral analysis of mPFC projector populations - downstream fluorescence & synaptophysin

Extended Data Fig. 3 | See next page for caption.

Extended Data Fig. 3 | Putative connection strength of mPFC projections to downstream targets, layer localization of projectors, and collateralization. a, Schematic of strategy in which anterogradely travelling virus was injected into the prelimbic and infralimbic subregions of the mPFC and fluorescence was quantified in several downstream brain regions. **b**, Orange boxes represent approximate locations of fluorescence quantification, as a proxy for connection strength. $n = 3$ rats. **c**, **d**, Representative images (**c**) and quantification of fluorescence (**d**) in the mPFC and downstream targets in the rat. **e**, Microinjections of CTB conjugated to fluorescent proteins (Alexa Fluor 488, Alexa Fluor 555 or Alexa Fluor 647, counterbalanced) were placed in the dPAG and NAc to retrogradely label the cell bodies of projection neurons in the rat mPFC ($n = 3$ rats). **f**, Representative confocal images of CTB injections in the NAc and dPAG of the rat. **g**, Representative confocal image of retrogradely labelled neurons in the rat mPFC. **h**, As a population, only 11 out of 1,679 CTB$^+$ neurons in the mPFC were dual-labelled. **i**, Fluorescence quantification of retrogradely labelled mPFC–dPAG and mPFC–NAc neurons revealed differences in cell-body location across cortical layers in the rat mPFC. **j**, In the rat, dPAG projectors predominantly originate from deep layer 5, whereas NAc projectors are located in both superficial layers 2/3 and deep layer 5. **k**, Microinjections of CTB conjugated to fluorescent proteins were placed in the dPAG and NAc to retrogradely label the cell bodies of projection neurons in the mouse mPFC. **l**, Representative confocal images of CTB injections in the NAc and dPAG of the mouse ($n = 3$ mice). **m**, Representative confocal image of retrogradely labelled neurons in the mouse mPFC. **n**, As a population, only 17 out of 458 CTB$^+$

neurons in the mPFC were dual-labelled. **o**, Fluorescence quantification of retrogradely labelled mPFC–dPAG and mPFC–NAc neurons revealed differences in cell-body location across cortical layers in the mouse mPFC. **p**, In the mouse, dPAG projectors predominantly originate from deep layer 5, whereas NAc projectors are located in both superficial layers 2/3 and deep layer 5. **q**, Schematic of viral strategy to explore downstream fluorescence from mPFC–NAc::eYFP ($n = 3$ rats) and mPFC–dPAG::eYFP ($n = 3$ rats) projectors. **r**, Quantification of fluorescence in the mPFC and downstream brain regions originating from mPFC–dPAG::eYFP and mPFC–NAc::eYFP neurons. **s**, **t**, Representative confocal images from a mPFC–dPAG::eYFP subject (**s**) and a mPFC–NAc::eYFP subject (**t**). **u**, Schematic of viral strategy to explore downstream terminals from mPFC–NAc::synaptophysin ($n = 3$ mice) and mPFC–dPAG::synaptophysin ($n = 3$ mice) projectors. **v**, Quantification of fluorescence in the mPFC and downstream brain regions originating from mPFC–dPAG::synaptophysin and mPFC–NAc::synaptophysin neurons. **w**, **x**, Representative confocal images from a mPFC–dPAG::synaptophysin subject (**w**) and a mPFC–NAc::synaptophysin subject (**x**). BLA, basolateral amygdala; agIN, agranular insula; cl, claustrum; dStr, dorsal striatum (medial); LH, lateral hypothalamus; LS, lateral septum; PHA, posterior hypothalamic area; PVT, paraventricular nucleus of the thalamus; vPAG, ventral periaqueductal grey. Rat and mouse brains in this figure have been reproduced with permission from Paxinos and Watson, 2006[53], and Paxinos and Franklin, 2004[54], respectively. Error bars and dashed lines represent s.e.m. Scale bars, 50 μm.
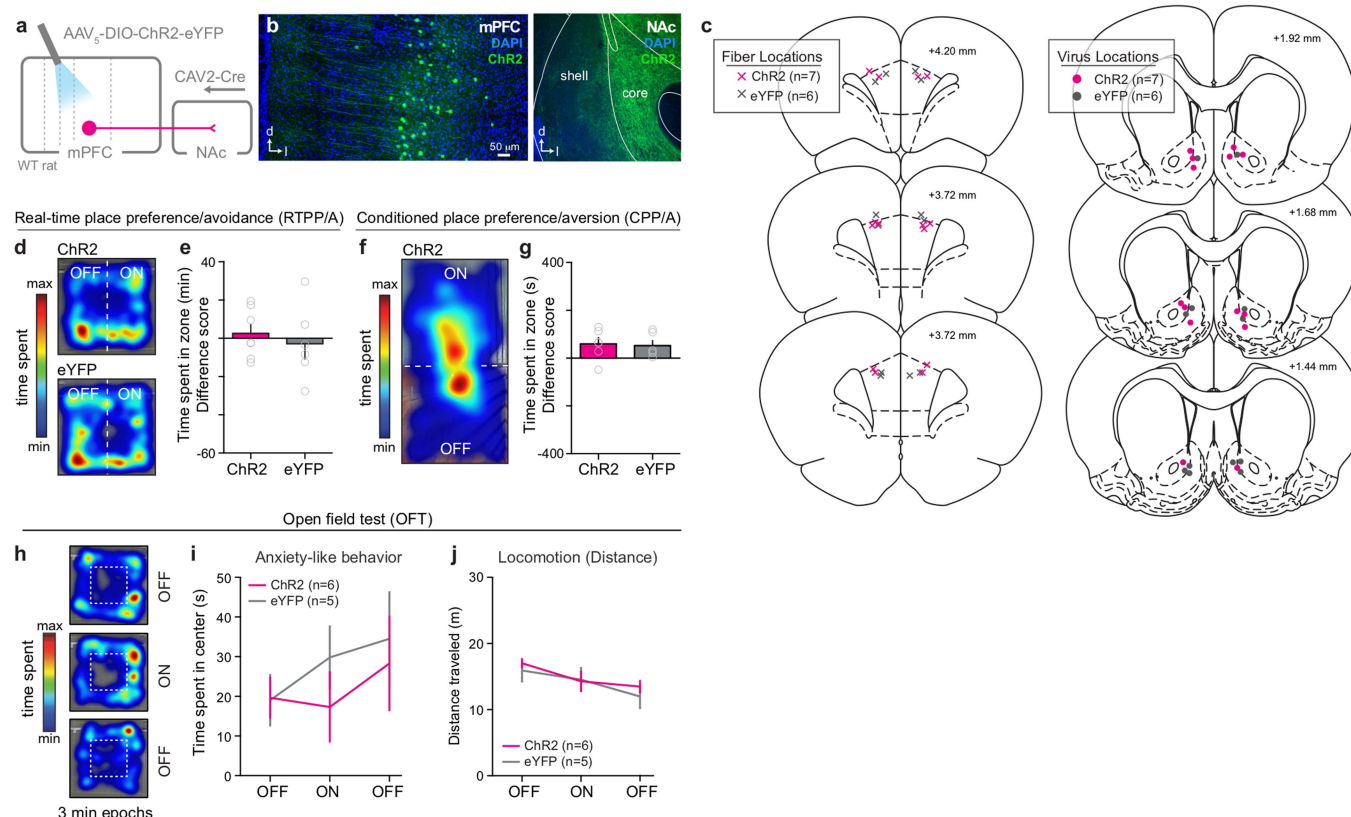
Extended Data Fig. 4 | mPFC–NAc photostimulation does not support place preference or aversion. a, Schematic of viral transduction strategy to achieve optogenetic control of rat mPFC neurons projecting to the NAc. **b**, Representative image of NAc-projecting mPFC neurons expressing ChR2 (left) and ChR2$^+$ terminals in the NAc (right). **c**, Histological verification of bilateral optical-fibre implant locations above the mPFC and virus injection locations in the NAc. **d**, Representative locomotor heat maps of mPFC–NAc::ChR2 (top) and mPFC–NAc::eYFP (bottom) subjects in the RTPP/A assay. **e**, Optogenetic stimulation of mPFC–NAc neurons did not evoke real-time place avoidance or preference in mPFC–NAc::ChR2 animals ($n = 7$ rats), compared to mPFC–NAc::eYFP controls ($n = 6$ rats), measured by difference score (minutes spent in the ON zone – minutes spent in OFF zone). Two-tailed unpaired t-test,

$t_{11} = 0.5549$, $P = 0.5901$. **f**, Representative locomotor heat map of mPFC–NAc::ChR2 subject in CPP/A assay. **g**, Optogenetic stimulation of mPFC–NAc neurons did not evoke real-time place aversion or preference in mPFC–NAc::ChR2 animals ($n = 6$ rats), compared to mPFC–NAc::eYFP controls ($n = 6$ rats). Two-tailed unpaired t-test, $t_{10} = 0.2143$, $P = 0.8346$. **h**, Representative locomotor heat maps of a mPFC–NAc::ChR2 subject during 3 min OFF–ON–OFF epochs during the open-field test. **i, j**, Optical activation of mPFC–NAc::ChR2 ($n = 6$ rats) did not change time spent in the centre region compared to eYFP controls ($n = 5$ rats) (**i**; two-way repeated measures ANOVA, $F_{2,18} = 0.74$, $P = 0.4913$), or general locomotor activity (**j**; two-way repeated measures ANOVA, $F_{2,18} = 0.61$, $P = 0.5532$). Data are mean ± s.e.m. The rat brains in this figure were reproduced with permission from Paxinos and Watson, 2006[53].
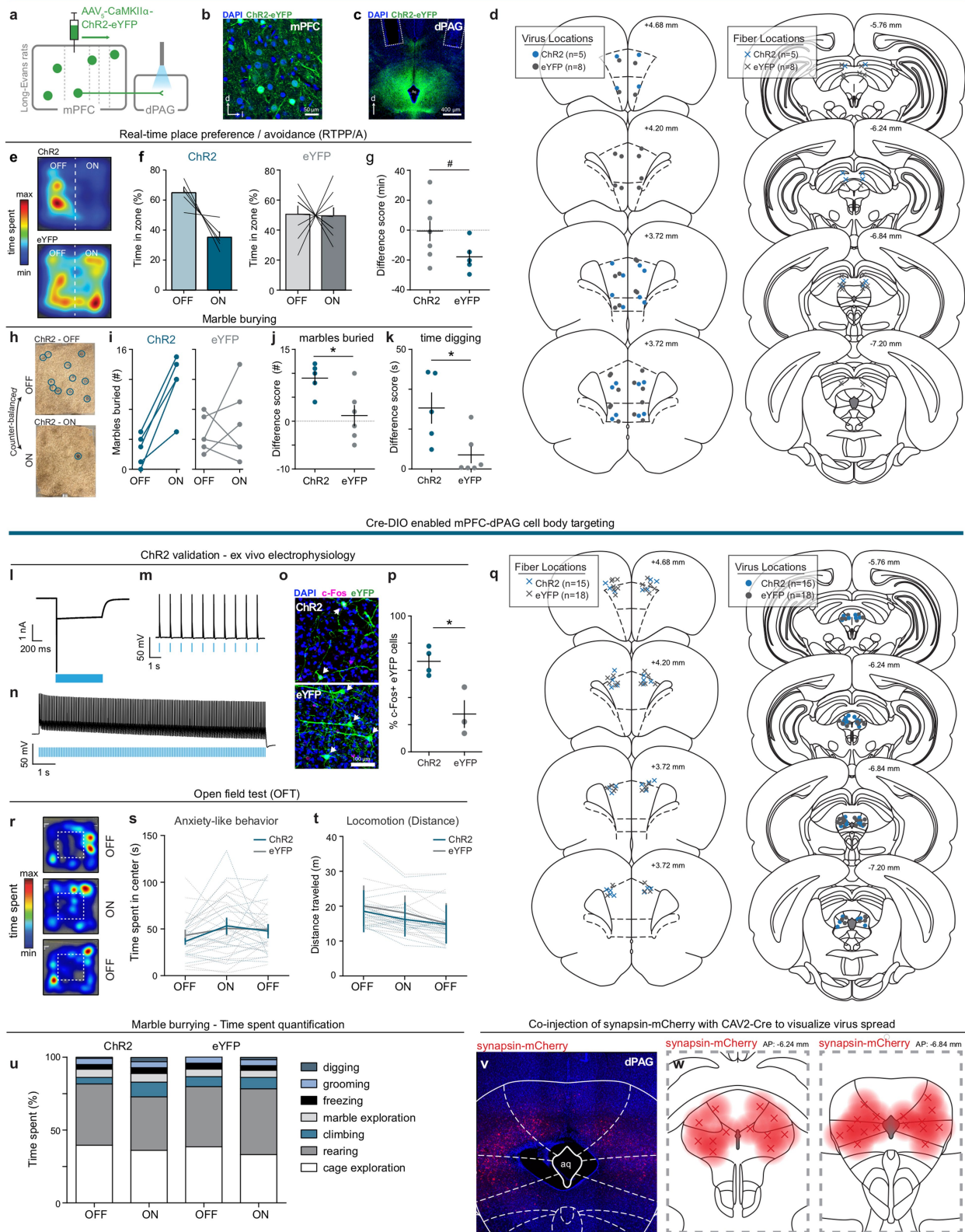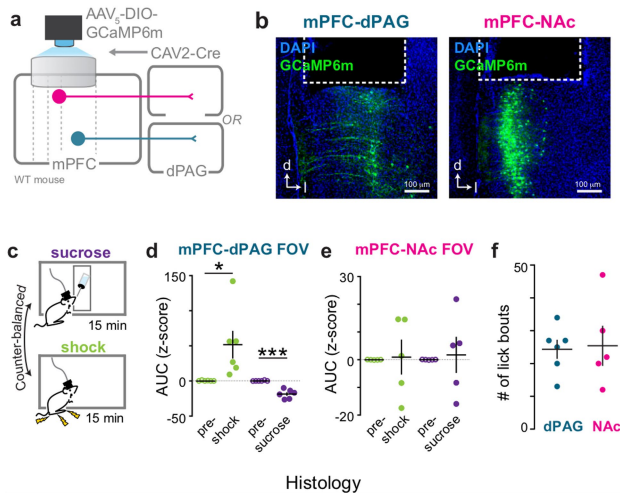
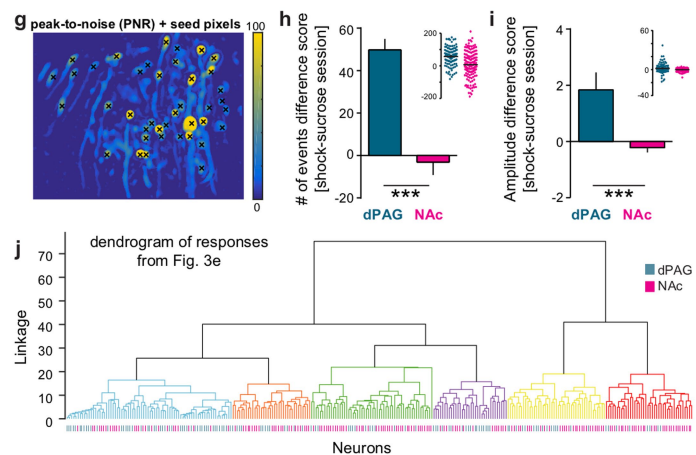Extended Data Fig. 5 | See next page for caption.

Extended Data Fig. 5 | Activation of mPFC terminals in the dPAG increases marble burying and activation of mPFC–dPAG cell bodies does not affect anxiety-like behaviour. a, Schematic of viral strategy to achieve optogenetic control of ChR2-expressing mPFC terminals in the dPAG. **b, c**, Representative image of ChR2$^+$ neurons in the mPFC (**b**) and ChR2$^+$ terminals in the dPAG (**c**) (optic fibre lesions indicated by dashed lines). **d**, Histological verification of bilateral virus injection locations in the mPFC and bilateral optic fibre implant locations above the dPAG. **e**, Representative locomotor heat maps of mPFC–dPAG::ChR2 (top) and mPFC–dPAG::eYFP control subject (bottom) in the RTPP/A assay. **f**, Percent of time spent in the ON and OFF zones of the arena in mPFC–dPAG::ChR2 and mPFC–dPAG::eYFP subjects. **g**, Optogenetic stimulation of mPFC terminals in the dPAG resulted in a trend towards avoidance in the RTPA assay in mPFC–dPAG::ChR2 animals ($n = 5$ rats), compared with mPFC–dPAG::eYFP controls ($n = 8$ rats). Two-tailed unpaired t-test, $t_{11} = 1.830$, $^\#P = 0.0944$. **h**, Representative arena of mPFC–dPAG::ChR2 animal after marble-burying assay when optical stimulation was OFF (top) and ON (bottom). **i**, Number of marbles buried in mPFC–dPAG::ChR2 ($n = 5$ rats) and mPFC–dPAG::eYFP ($n = 6$ rats) during OFF and ON sessions. **j, k**, Optical stimulation of mPFC–dPAG neurons resulted in more marbles buried by mPFC–dPAG::ChR2 animals, compared with mPFC–dPAG::eYFP controls (**j**; two-tailed unpaired t-test, $t_9 = 2.839$, $*P = 0.0194$) and more time digging (**k**; one-tailed unpaired t-test, $t_9 = 2.775$, $*P = 0.0108$). **l**, Functional ChR2 expression in mPFC–dPAG neurons was verified by targeted ex vivo whole-cell patch-clamp electrophysiology. Recording from a ChR2-expressing mPFC–dPAG neuron in voltage-clamp mode showing sustained inward current elicited by a 1-s pulse of 470-nm light.

m, n, In current-clamp mode, action potentials were elicited by 1-Hz (**m**) and 20-Hz light trains (**n**). 470 nm, 5-ms pulse duration. **o**, Representative confocal images of mPFC–dPAG::ChR2 (top) and mPFC–dPAG::eYFP expressing neurons showing immediate early gene (c-Fos) expression following 5 min blue (473 nm) light exposure (20 Hz, 5-ms pulse duration, 15 mW). **p**, Laser light stimulation (473 nm) enhanced the number of c-Fos-positive ChR2-expressing mPFC–dPAG neurons compared with control mPFC–dPAG::eYFP neurons. mPFC–dPAG::ChR2, $n = 4$ rats; mPFC–dPAG::eYFP, $n = 3$ rats; two-tailed unpaired t-test, $t_5 = 3.707$, $*P = 0.014$. **q**, Histological verification of bilateral optical-fibre implant locations above the mPFC and virus injection locations in the dPAG for mPFC–dPAG::ChR2/eYFP-expressing rats. **r**, Representative locomotor heat maps of a mPFC–dPAG::ChR2 subject during 3 min OFF–ON–OFF epochs in the open-field test. **s, t**, Optical activation of mPFC–dPAG::ChR2 ($n = 15$ rats) did not change time spent in the centre region compared to eYFP controls (**s**; $n = 18$ rats, two-way repeated measures ANOVA, group $\times$ epoch, $F_{2,62} = 0.37$, $P = 0.69$), or general locomotor activity (**t**; distance travelled, two-way repeated measures ANOVA, group $\times$ epoch interaction, $F_{2,62} = 0.9412$, $P = 0.3957$). **u**, Quantification of behaviours (percentage of time engaging) during marble-burying assay. **v**, Representative confocal image of viral spread in the PAG, visualized by co-injection of AAV$_5$-hSyn-mCherry (hSyn, synapsin, red) with CAV2-Cre in a subset of mPFC–dPAG::ChR2/eYFP expressing rats. **w**, Illustration of reconstructed injection locations and spread in co-injected subjects. $n = 14$ total, 7 ChR2, 7 eYFP. Error bars indicate s.e.m. The rat brains in this figure were reproduced with permission from Paxinos and Watson, 2006[53].
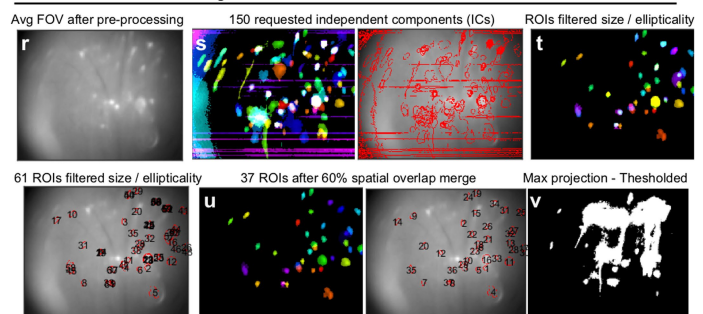
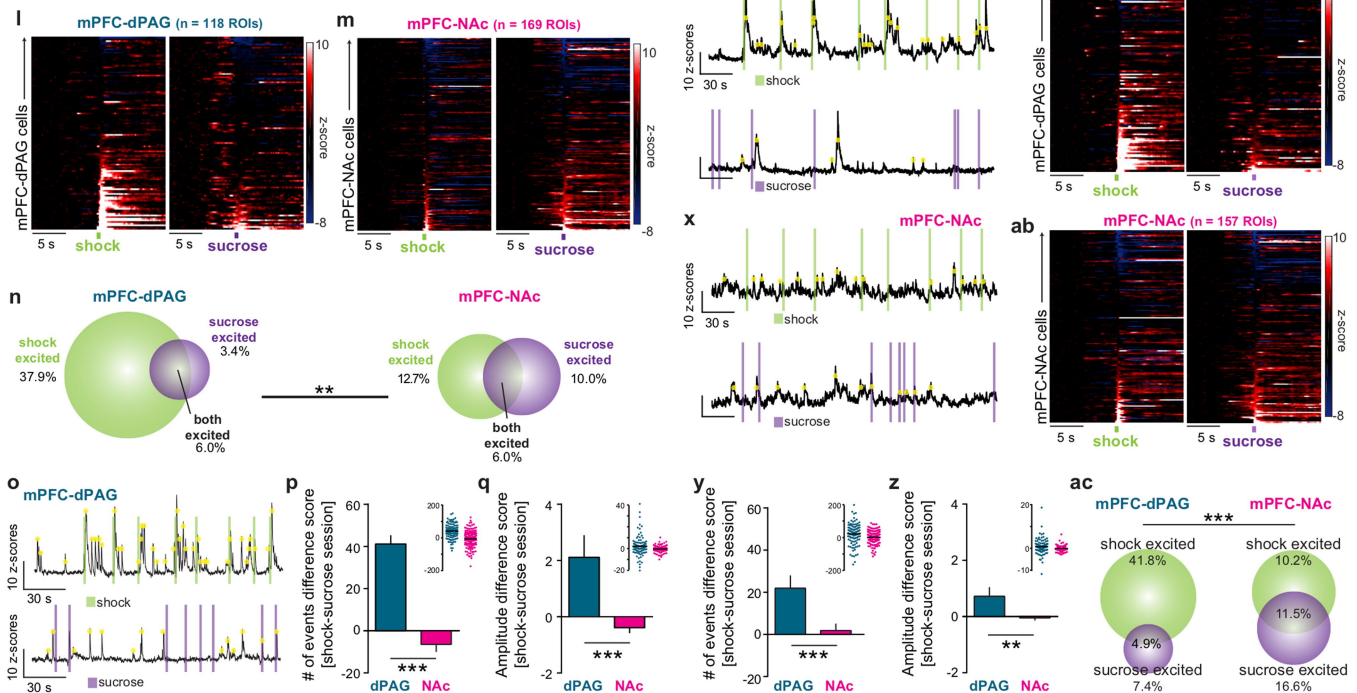## Additional FOV & behavioral results

Additional CNMF-E results

Histology

Results using "Non-ROI thresholded subtraction" method

Results using CNMF-E with removal of non-negative constraints

Extended Data Fig. 6 | See next page for caption.

Extended Data Fig. 6 | Analysis and additional data from epifluorescent calcium imaging experiments during sucrose and shock delivery.
a, Schematic of strategy for monitoring neuronal activity in mPFC–dPAG and mPFC–NAc neurons using in vivo calcium imaging.
b, Representative confocal images of mPFC–NAc::GCaMP6m (left) and mPFC–dPAG::GCaMP6m neurons (right) underneath GRIN lenses (dashed lines). **c**, Dynamic calcium fluctuations were monitored during a 15-min recording session in which mice were allowed to self-administer sucrose via a sucrose lickometer or had random, unsignalled foot shocks delivered. **d**, As a population, mPFC–dPAG::GCaMP6m ($n = 6$ mice) were activated to foot shock (green, two-tailed paired t-test, $t_5 = 2.616$, $*P = 0.0473$) or inhibited by the initiation of a sucrose bout (purple, two-tailed paired t-test, $t_5 = 6.982$, $***P = 0.0009$) as measured by the bulk fluorescence across the entire FOV (-3 to 0 s, pre-shock/sucrose; 0–3 s, shock/sucrose). **e**, As a population, mPFC–NAc::GCaMP6m ($n = 5$ mice) were not responsive to foot shock (green, two-tailed paired t-test, $t_4 = 0.1520$, $P = 0.8866$) or the initiation of a sucrose bout (purple, two-tailed paired t-test, $t_4 = 0.2678$, $P = 0.8021$) (-3 to 0 s, pre-shock/sucrose; 0–3 s, shock/sucrose). **f**, mPFC–dPAG::GCaMP6m and mPFC–NAc::GCaMP6m mice did not differ in the number of lick bouts initiated during the sucrose session. Two-tailed unpaired t-test, $t_9 = 0.1666$, $P = 0.8714$. **g**, Peak-to-noise heat map generated from a representative FOV with seed pixels overlaid (black X). **h**, mPFC–dPAG::GCaMP6m neurons ($n = 118$ ROIs) had more frequent calcium transients than mPFC–NAc::GCaMP6m neurons ($n = 169$ ROIs) during the shock session. Number of events difference score (shock − sucrose): dPAG Mdn, 51.5; NAc Mdn, −6. Two-tailed Mann–Whitney test, $U = 5,840$, $***P < 0.0001$. **i**, mPFC–dPAG::GCaMP6m neurons had higher amplitude transients than mPFC–NAc::GCaMP6m neurons during the shock session. Amplitude of events difference score (shock − sucrose): dPAG Mdn, 0.9031; NAc Mdn, −0.3549. Mann–Whitney test, $U = 6,672$, $***P < 0.0001$. **j**, Dendrogram of agglomerative hierarchical clustering. Different colours represent clusters based on average responses per ROI to footshock and sucrose. **k**, Histologically verified locations of GRIN lens implants. **l–ac**, In addition to using CNMF-E, imaging data were analysed using two other approaches: 1) a modified constrained CNMF-E algorithm considering calcium fluctuations can have negative transients, associated with a decrease in firing[24,55] (for the approach, we did not constrain temporal components to >0) and 2) a ROI-based method (that is, 'non-ROI', **r–ac**). **l**, **m**, Calcium signals were extracted from individual ROIs and the average calcium traces per ROI were aligned to shock and sucrose bout onset for mPFC–NAc::GCaMP6m (**l**) and mPFC–dPAG::GCaMP6m recordings (**m**). **n**, The distribution of shock- and sucrose-excited cells for mPFC–dPAG::GCaMP6m neurons was different from mPFC–NAc::GCaMP6m neurons. $\chi^2 = 10.95$, $**P = 0.0042$.
o, Representative calcium traces from a mPFC–dPAG::GCaMP6m neuron during shock (top) and sucrose (bottom) recording sessions. Individual calcium transients (yellow dots) were identified and quantified.
p, mPFC–dPAG::GCaMP6m neurons ($n = 118$ ROIs) had more frequent calcium transients than mPFC–NAc::GCaMP6m neurons ($n = 169$ ROIs) during the shock session. Number of events difference score (shock − sucrose): dPAG Mdn, 43; NAc Mdn, −3. Two-tailed Mann–Whitney test, $U = 4,373$, $***P < 0.0001$. **q**, mPFC–dPAG::GCaMP6m neurons had higher amplitude calcium transients compared to mPFC–NAc::GCaMP6m neurons during the shock session. Amplitude of events difference score (shock − sucrose): dPAG Mdn, 1.329; NAc Mdn, −0.2459. Two-tailed Mann–Whitney test, $U = 7,164$, $***P < 0.0001$.
r, Mean t-projection image of the entire FOV through the relay lens after image pre-processing. Recordings were converted to changes in fluorescence compared to background fluorescence $(F - F_0)/F_0$ using the mean t-projection image as reference (F_0). **s**, Calcium signals arising from ROIs were identified using independent and principal component analyses (PCA/ICA). **t**, Identified PCA/ICA filters were thresholded at their half-maximum values to define possible ROIs and were screened for neuronal morphology. ROIs were only accepted if the threshold filters included only on contiguous region with an eccentricity of <0.85 and an area between 30–350 pixels. In this example, 61 ROIs (of the original 150 independent components (ICs)) met these criteria. **u**, Accepted ROI filters were then merged if their areas overlapped by more than 60%. In this example, 24 ROIs were merged for a remaining total of 37 valid ROIs. **v**, To acquire the non-ROI thresholded image for background subtraction, max z projections of individual recordings were created and thresholded to separate ROIs and their processes from the rest of the FOV. Average signal from the remaining pixels was used as a proxy for the whole-field changes in fluorescence, and regressed from the signal extracted from each ROI. **w**, **x**, Calcium transients (yellow dots) within individual mPFC–dPAG::GCaMP6m neurons (**w**) and mPFC–NAc::GCaMP6m neurons (**x**) were quantified (representative traces). **y**, mPFC–dPAG::GCaMP6m neurons ($n = 113$ of 118 ROIs) had more frequent calcium transients than mPFC–NAc::GCaMP6m neurons ($n = 157$ ROIs) during the shock session. Difference score (shock − sucrose): dPAG Mdn, 30; NAc Mdn, 6. Two-tailed Mann–Whitney test, $U = 6,392$, $***P < 0.0001$. **z**, mPFC–dPAG::GCaMP6m neurons had calcium transients of larger amplitude than mPFC–NAc::GCaMP6m neurons during the shock session. Difference score (shock − sucrose): dPAG Mdn, 0.5158; NAc Mdn, −0.0615. Two-tailed Mann–Whitney test, $U = 7,065$, $**P = 0.0044$. **aa**, **ab**, Average calcium traces per cell for mPFC–dPAG::GCaMP6m neurons (**aa**) and mPFC–NAc::GCaMP6m neurons (**ab**) were aligned to shock (left) and sucrose bout (right). **ac**, The distribution of shock- and sucrose-excited cells for mPFC–dPAG::GCaMP6m ($n = 118$ ROIs) neurons was different from that for mPFC–NAc::GCaMP6m neurons ($n = 157$ ROIs). $\chi^2 = 32.33$, $***P < 0.0001$. Error bars and '+' indicate s.e.m. Scale bar, 100 μm. The mouse brains in this figure were reproduced with permission from Paxinos and Franklin, 2004[54].

Sholl analysis on reconstructed mPFC-NAc and mPFC-dPAG neurons

dopamine receptor localization on projectors
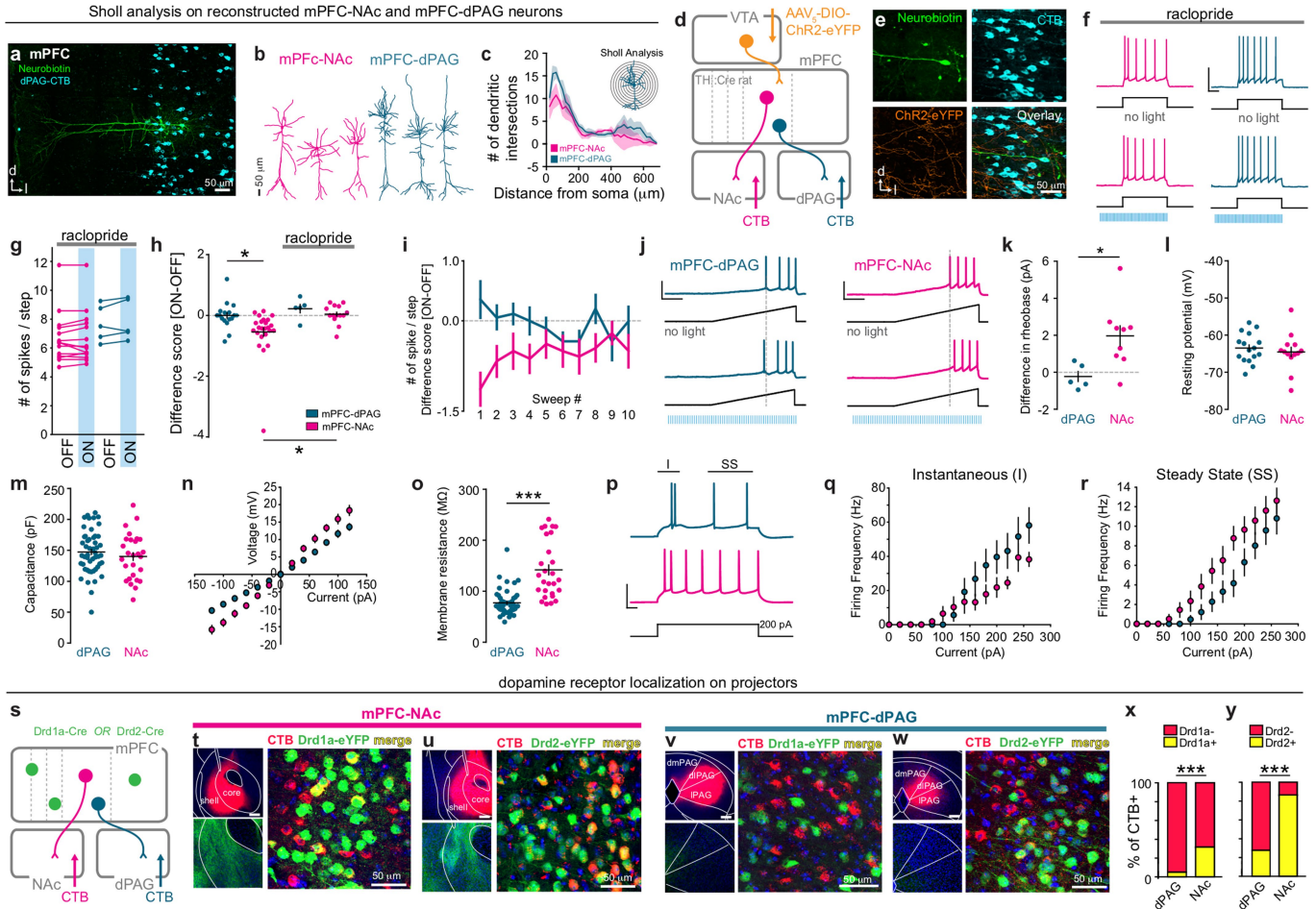
Extended Data Fig. 7 | VTA^{DA} effects on mPFC projectors across time and their properties. a, Representative confocal image of mPFC–dPAG labelled neurons. **b**, Representative examples of reconstructed mPFC–NAc and mPFC–PAG neurons. **c**, Sholl analysis of mPFC–NAc ($n=4$ cells) and mPFC–dPAG ($n=4$ cells) subpopulations. **d**, Schematic of viral strategy to optically manipulate ChR2-expressing VTA^{DA} terminals in the mPFC and record from dPAG- and NAc-projectors retrogradely labelled with CTB using ex vivo electrophysiology. **e**, Representative images of a recorded mPFC–dPAG neuron (neurobiotin$^+$ and CTB$^+$) surrounded by ChR2–eYFP$^+$ VTA^{DA} terminals. **f**, Representative traces of a mPFC–dPAG and mPFC–NAc neuron during a current step without (top) and with (bottom) optogenetic activation of VTA^{DA} terminals in the presence of type D2-type dopamine receptor blockade by bath-applied raclopride. **g**, The change in spike number with optical stimulation (ON–OFF) recorded from mPFC–dPAG ($n=5$ cells) and mPFC–NAc neurons ($n=14$ cells) in the presence of D2-receptor antagonism. **h**, The change in spike number with optical stimulation (ON–OFF) was different between mPFC–dPAG ($n=17$ cells) and mPFC–NAc neurons ($n=24$ cells) and was blocked by D2-receptor antagonism. One-way ANOVA, $F_{3,56}=5.343$, $P=0.0026$; Bonferroni multiple comparisons tests: dPAG vs NAc, $*P=0.0040$; NAc vs NAc + raclopride, $*P=0.0034$. **i**, Change in the number of spikes per step with optical stimulation (ON–OFF) for individual sweeps. mPFC–NAc neurons exhibited a more robust decrease in spike number during VTA^{DA} terminal stimulation during the first few sweeps, an effect that diminished in later sweeps. **j**, Representative traces showing firing elicited in mPFC–dPAG and mPFC–NAc neurons in response to current ramp with and without VTA^{DA} terminal stimulation (grey dashed line indicates time of first action potential without optical stimulation). Scale bars, 50 mV, 500 ms. **k**, Optical stimulation of VTA^{DA} terminals increased the current required to elicit an action potential (rheobase) in NAc projectors. The change in rheobase with optical stimulation (ON–OFF) was different between dPAG projectors ($n=5$ cells) and NAc projectors ($n=9$ cells). Two-tailed

unpaired t-test, $t_{12}=2.669$, $P=0.0205$. **l, m**, Neither resting membrane potential (mPFC–dPAG, $n=16$ cells; mPFC–NAc, $n=13$ cells) (**l**) nor capacitance (**m**) differed between dPAG-projectors ($n=50$ cells) and NAc-projectors ($n=27$ cells). Resting membrane potential: two-tailed unpaired t-test, $t_{27}=0.6265$, $P=0.5363$; capacitance: two-tailed unpaired t-test, $t_{75}=0.8643$, $P=0.3902$. **n**, The current-voltage ($I–V$) relationship of mPFC–dPAG ($n=16$ cells) and mPFC–NAc ($n=13$ cells) neurons obtained by applying a series of current steps in voltage-clamp mode. Two-way ANOVA, $F_{12,324}=10.16$, $P<0.0001$. **o**, The membrane resistance was significantly greater in NAc projectors ($n=27$ cells) compared to dPAG projectors ($n=50$ cells). Two-tailed unpaired t-test, $t_{75}=7.030$, $***P<0.0001$. **p**, Representative traces showing action potential firing in mPFC–dPAG and mPFC–NAc neurons in response to a depolarizing current step. Scale bars, 50 mV, 500 ms. **q, r**, Instantaneous (I) (**q**) and steady-state (SS) (**r**) firing frequency in dPAG and NAc projectors in response to increasing current steps. **s**, Schematic of strategy for identifying dopamine type 1 receptor (D1) and dopamine type 2 receptor (D2) on mPFC-projector populations using transgenic mice (Drd1a-Cre ($n=3$ mice) and Drd2-Cre ($n=3$ mice)), retrograde labelling, and Cre-dependent eYFP recombination. **t, u**, Representative confocal images of NAc CTB injections sites (upper left), mPFC terminal fluorescence (lower left), and mPFC–NAc cell bodies (right) in a Drd1a-Cre::eYFP mouse (**t**) and Drd2-Cre::eYFP mouse (**u**). **v, w**, Representative confocal images of dPAG CTB injections sites (upper left), mPFC terminal fluorescence (lower left), and mPFC–dPAG cell bodies (right) in a Drd1a-Cre::eYFP mouse (**v**) and a Drd2-Cre::eYFP mouse (**w**). **x**, 5% of mPFC–dPAG CTB$^+$ neurons were Drd1a$^+$ (19/378), whereas 31.5% of mPFC–NAc CTB$^+$ neurons were co-labelled as Drd1a$^+$ (151/479) (D1 $\chi^2=93.29$, $***P<0.0001$). **y**, 27.6% of mPFC–dPAG CTB$^+$ neurons were Drd2$^+$ (74/342), whereas 86.3% of mPFC–NAc CTB$^+$ neurons were co-labelled as Drd2$^+$ (414/480) (D2 $\chi^2=345.6$, $***P<0.0001$). Error bars, shading, and '+' represent s.e.m.
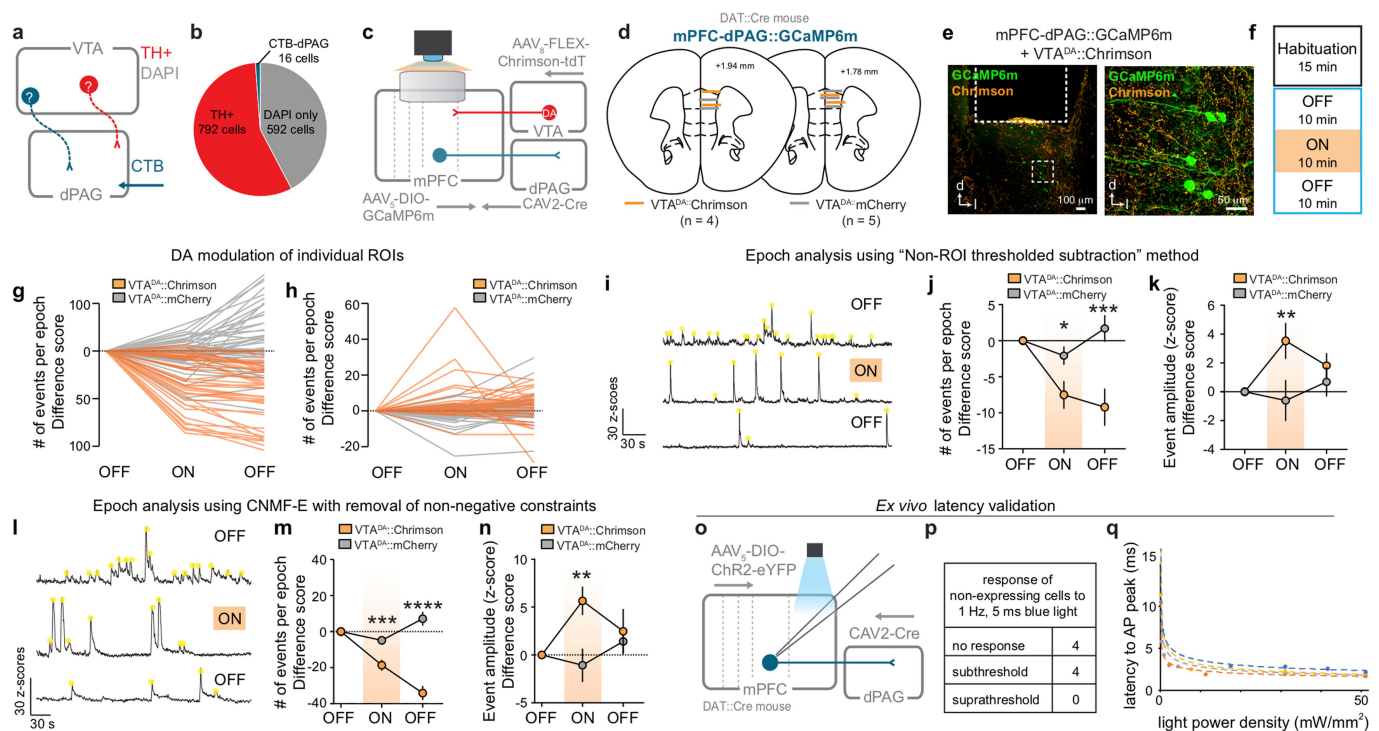
Extended Data Fig. 8 | Investigation of VTA projections to the dPAG for simultaneous epifluorescent imaging in mPFC–dPAG neurons and excitation of VTA^{DA} terminals. a, To verify that VTA neurons do not project to the dPAG (to allow for CAV2-Cre mediated GCaMP6m expression in dPAG neurons and simultaneous expression of the excitatory opsin Chrimson in VTA^{DA} neurons in DAT::Cre mice), VTA slices were immunostained for tyrosine hydroxylase (TH) in rats injected with the retrograde tracer CTB in the dPAG. **b**, Of 1,400 DAPI$^+$ cells counted in the VTA, 792 (56%) were TH$^+$, 16 (1.1%) were CTB$^+$, and 0 were TH$^+$ and CTB$^+$. The lack of CTB$^+$ cells suggests that VTA does not make a prominent projection to the dPAG. **c**, Schematic of strategy to simultaneously image fluorescent calcium activity in mPFC–dPAG::GCaMP6m neurons and activate VTA^{DA}–mPFC. **d**, Histological verification of GRIN lens locations in the mPFC in mPFC–dPAG::GCaMP6m × VTA^{DA}::Chrimson subjects and control mPFC–dPAG::GCaMP6m × VTA^{DA}::mCherry subjects. **e**, Representative confocal images of mPFC–dPAG::GCaMP6m and VTA^{DA}::Chrimson expression in the mPFC. **f**, Schematic of experimental design. During the ON epoch, a 590-nm LED stimulated Chrimson expressing VTA^{DA}–mPFC (20 Hz, 60 pulses of 5 ms, every 30 s). **g**, Individual ROI transient frequency analysed with CNMF-E. **h**, Individual ROI transient amplitude analysed with CNMF-E. **i–k**, Data analysed using a non-ROI thresholded subtraction method (Chrimson: $n = 4$ mice, 44 ROIs; mCherry: $n = 5$ mice, 50 ROIs). **i**, Representative traces from a mPFC–dPAG::GCaMP6m neuron during the OFF–ON–OFF recording epochs. Calcium transients (yellow dots) for each neuron were identified and quantified. **j**, VTA^{DA}–mPFC stimulation decreased the average calcium event frequency per neuron, during both the ON and second OFF epochs. Data normalized to first OFF epoch; two-way repeated measure ANOVA, $F_{2,184} = 9.209$, $P = 0.0002$; Bonferroni multiple comparisons tests, $P < 0.05$. **k**, VTA^{DA}–mPFC stimulation increased the average calcium event amplitude per cell during the ON epoch, an effect that recovered in the second OFF epoch. Data normalized to first OFF epoch; two-way repeated measure ANOVA, $F_{2,184} = 3.756$, $P = 0.0252$; Bonferroni multiple comparisons tests: $P < 0.05$. **l–n**, Data analysed using CNMF-E with removal of non-negative temporal constraints. Chrimson: $n = 4$ mice, 44 ROIs; mCherry: $n = 5$ mice; 50 ROIs. **l**, Representative traces from a mPFC–dPAG::GCaMP6m neuron during each 10 min OFF–ON–OFF recording epoch. Calcium transients (yellow dots) for each neuron were identified and quantified. **m**, VTA^{DA}–mPFC stimulation decreased the average calcium event frequency per neuron, during both the ON and second OFF epochs. Data normalized to first OFF epoch; two-way repeated measure ANOVA, $F_{2,184} = 43.62$, $P < 0.0001$; Bonferroni multiple comparisons tests: $P < 0.05$. **n**, VTA^{DA}–mPFC stimulation increased the average calcium event amplitude per cell during the ON epoch, an effect that recovered in the second OFF epoch. Data normalized to first OFF epoch; two-way repeated measure ANOVA, $F_{2,184} = 3.50$, $P = 0.0322$; Bonferroni multiple comparisons tests: $P < 0.05$. **o**, Schematic of viral strategy to optically manipulate ChR2-expressing VTA^{DA} terminals in the mPFC and record from mPFC–dPAG::ChR2 and non-expressing neighbouring neurons with ex vivo electrophysiology. **p**, Number of non-expressing cells with different responses to 1 Hz, 5-ms blue light delivery. **q**, Latency to action-potential peak for all ChR2-expressing cells plotted against light power density. Error bars represent s.e.m. The mouse brains in this figure were reproduced with permission from Paxinos and Franklin, 2004[54].
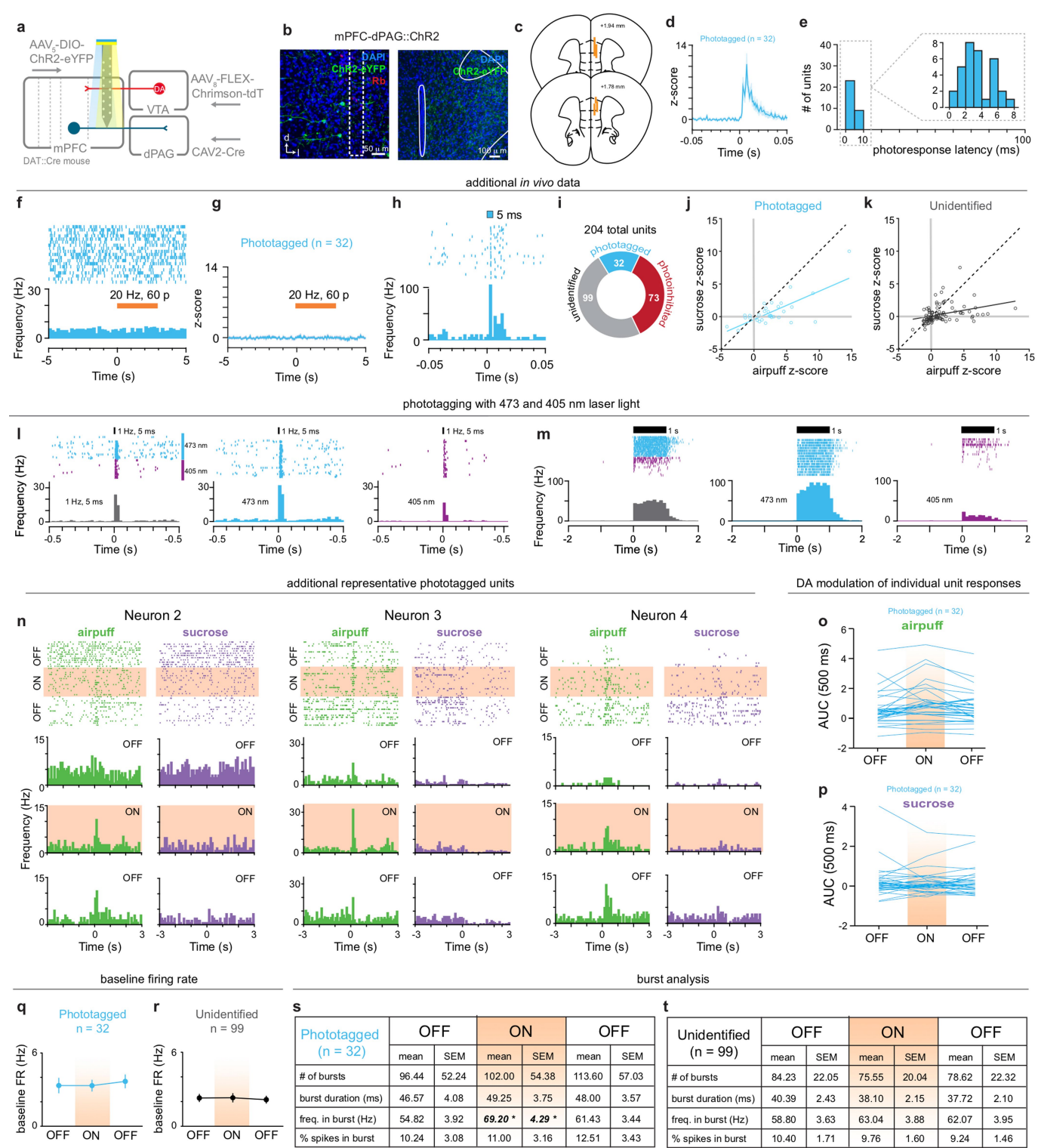
Extended Data Fig. 9 | See next page for caption.

Extended Data Fig. 9 | Additional data for head-fixed electrophysiological recordings. a, Schematic of strategy to manipulate VTA^{DA} terminals in the mPFC and optically identify mPFC–dPAG::ChR2 neurons using in vivo head-fixed electrophysiology. **b**, Representative image of recording track in the mPFC (Rb, red retrobeads) and ChR2–eYFP-expressing mPFC–dPAG neurons. Representative image of ChR2–eYFP-expressing terminals surrounding the PAG. **c**, Histologically verified locations of recording tracks for in vivo head-fixed electrophysiology experiments. **d**, Population z-score of all phototagged units aligned to 1 Hz, 5-ms pulse of 473 nm. **e**, Photoresponse latencies showing <8 ms response latency from all 32 mPFC–dPAG::ChR2 units. **f, g**, PSTH from representative phototagged unit (**f**) and population z-score showing no response (**g**) to 20 Hz, 60 pulses of 593-nm laser light used for VTA^{DA}::Chrimson terminal activation. **h**, Representative PSTH of the firing rate in response to the onset of 5-ms pulse of 473-nm laser light used for phototagging. **i**, 204 mPFC units were recorded ($n = 3$ mice, 5 recording sessions) and 32 phototagged units were identified as mPFC–dPAG projectors (blue), 73 were photoinhibited (red), and 99 remained unidentified (grey). **j, k**, Neural response magnitudes to airpuff (x axis) and sucrose (y axis) in phototagged (**j**; blue) and unidentified (**k**;

black) populations. **l, m**, In a subset of mice, both 405 and 473-nm laser light were used for phototagging. **l**, Representative phototagged unit showing faithful responses to 1 Hz, 5-ms pulses of both 473 and 405-nm light. **m**, Representative phototagged unit showing blunted response to 1 s of 405-nm, compared to 473-nm light. **n**, Representative PSTHs of photoidentified mPFC–dPAG units aligned to airpuff (green) and sucrose (purple). Histograms show neural responses in the OFF–ON–OFF epochs. **o, p**, Individual neural responses (AUC (0–500 ms post-stimulus presentation)) of every phototagged unit ($n = 32$ units) to airpuff (**o**) and sucrose (**p**) in each of the three recording epochs (OFF–ON–OFF). **q, r**, VTA dopamine terminal stimulation in the mPFC did not change the baseline firing rate (FR) in the 3-s pre-stimulus windows in the phototagged (**q**; Friedman test, $\chi^2 = 2.472$, $P = 0.2905$) or unidentified (**r**; Friedman test, $\chi^2 = 0.4242$, $P = 0.8089$) populations. **s**, VTA^{DA} terminal activation increased the frequency within a burst in the phototagged population. **t**, VTA^{DA} terminal activation did not affect burst characteristics in the unidentified population. Error bars indicate s.e.m. The mouse brains in this figure were reproduced with permission from Paxinos and Franklin, 2004[54].
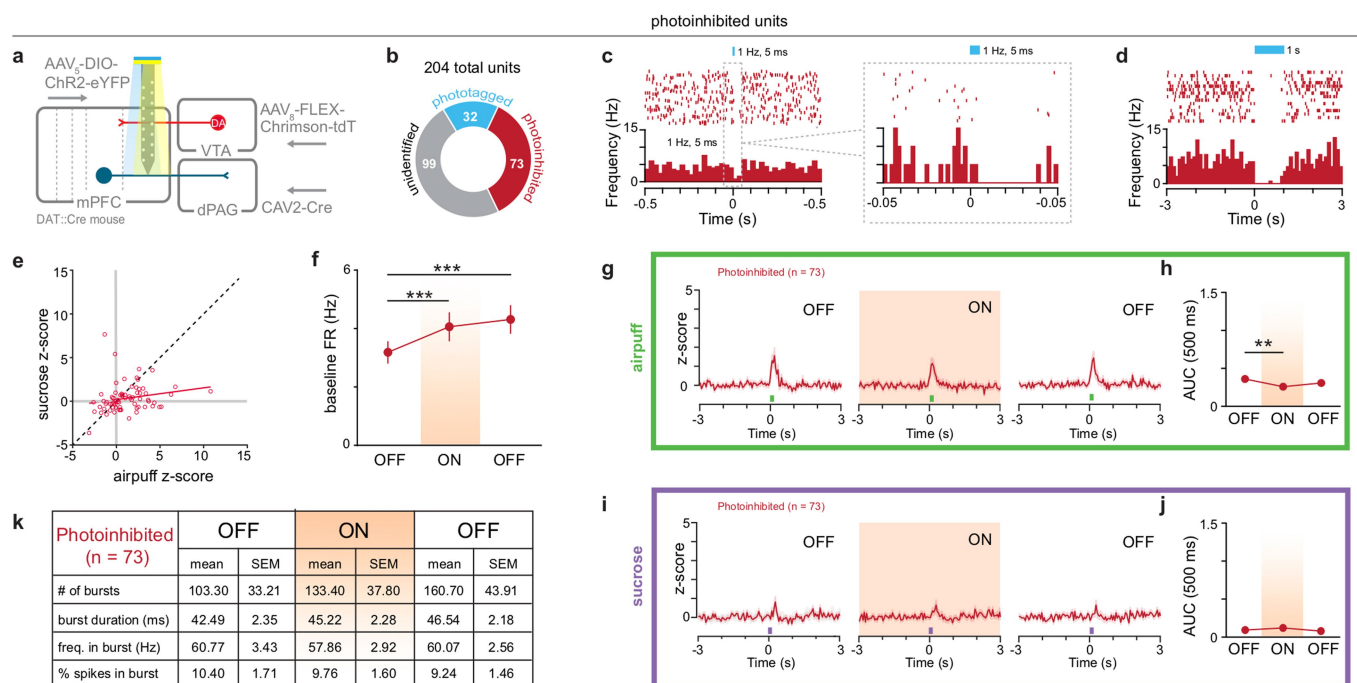
Extended Data Fig. 10 | Dopamine-attenuates responses to airpuff in photoinhibited mPFC neurons. a, Schematic of strategy to manipulate VTA^{DA} terminals in the mPFC and optically identify mPFC–dPAG::ChR2 neurons using in vivo head-fixed electrophysiology. $n = 3$ mice, 5 recording sessions. **b**, 35.8% of recorded units (73/204) were photoinhibited. **c, d**, Representative PSTHs of a photoinhibited unit in response to 1 Hz, 5 ms (**c**) and 1 s (**d**) of 473-nm light. **e**, Neural response magnitudes to airpuff (x axis) and sucrose (y axis) in photoinhibited (red) population. **f**, VTA^{DA} terminal stimulation in the mPFC increased the baseline firing rate in the 3-s pre-stimulus windows in the photoinhibited population ($n = 73$ units) during the ON and second OFF epochs

(Friedman test, $\chi^2 = 16.22$; $P = 0.0003$; Dunn's multiple comparisons tests, $P < 0.05$). **g**, Population z-score of photoinhibited units aligned to airpuff in each of the recording epochs. **h**, In photoinhibited neurons, VTA^{DA} terminal stimulation attenuated neural responses to airpuff (Friedman test, $\chi^2 = 8.329$, $P = 0.0155$; Dunn's multiple comparisons tests, $P < 0.05$). **i**, Population z-score of photoinhibited units aligned to sucrose in each of the recording epochs. **j**, In photoinhibited neurons, VTA^{DA} terminal stimulation did not affect neural responses to sucrose (Friedman test, $\chi^2 = 0.4492$, $P = 0.7988$; Dunn's multiple comparisons tests, $P > 0.05$. **k**, VTA^{DA} terminal activation did not affect burst characteristics in the photoinhibited population. Error bars and shading represent s.e.m.

natureresearch

Corresponding author(s):   Kay M. Tye (2016-08-10753D)

Reporting Summary

Nature Research wishes to improve the reproducibility of the work that we publish. This form provides structure for consistency and transparency in reporting. For further information on Nature Research policies, see Authors & Referees and the Editorial Policy Checklist.

Statistical parameters

When statistical analyses are reported, confirm that the following items are present in the relevant location (e.g. figure legend, table legend, main text, or Methods section).

n/a	Confirmed	
☐	☒	The exact sample size (n) for each experimental group/condition, given as a discrete number and unit of measurement
☐	☒	An indication of whether measurements were taken from distinct samples or whether the same sample was measured repeatedly
☐	☒	The statistical test(s) used AND whether they are one- or two-sided *Only common tests should be described solely by name; describe more complex techniques in the Methods section.*
☒	☐	A description of all covariates tested
☐	☒	A description of any assumptions or corrections, such as tests of normality and adjustment for multiple comparisons
☐	☒	A full description of the statistics including central tendency (e.g. means) or other basic estimates (e.g. regression coefficient) AND variation (e.g. standard deviation) or associated estimates of uncertainty (e.g. confidence intervals)
☐	☒	For null hypothesis testing, the test statistic (e.g. F, t, r) with confidence intervals, effect sizes, degrees of freedom and P value noted *Give P values as exact values whenever suitable.*
☒	☐	For Bayesian analysis, information on the choice of priors and Markov chain Monte Carlo settings
☐	☒	For hierarchical and complex designs, identification of the appropriate level for tests and full reporting of outcomes
☒	☐	Estimates of effect sizes (e.g. Cohen's d, Pearson's r), indicating how they were calculated
☐	☒	Clearly defined error bars *State explicitly what error bars represent (e.g. SD, SE, CI)*

Our web collection on statistics for biologists may be useful.

Software and code

Policy information about availability of computer code

Data collection	All data were collected with commercially available software reported in the Methods section for each experiment. More information is available upon request.
Data analysis	Data were analyzed with commercially available, open-source, and in-house custom code. Description of these methods are reported in the Methods section for each experiment. If descriptions were published elsewhere, full references are included throughout the Main and Extended text. Custom code is available upon request.

For manuscripts utilizing custom algorithms or software that are central to the research but not yet described in published literature, software must be made available to editors/reviewers upon request. We strongly encourage code deposition in a community repository (e.g. GitHub). See the Nature Research guidelines for submitting code & software for further information.

Data

All manuscripts must include a data availability statement. This statement should provide the following information, where applicable:

- Accession codes, unique identifiers, or web links for publicly available datasets
- A list of figures that have associated raw data
- A description of any restrictions on data availability

All data available upon request.

Field-specific reporting

Please select the best fit for your research. If you are not sure, read the appropriate sections before making your selection.

☒ Life sciences ☐ Behavioural & social sciences ☐ Ecological, evolutionary & environmental sciences

For a reference copy of the document with all sections, see nature.com/authors/policies/ReportingSummary-flat.pdf

Life sciences study design

All studies must disclose on these points even when the disclosure is negative.

Sample size	Sample sizes were not predetermined and based on similar reports in the literature. This is reported in the Methods for each experiment where appropriate.
Data exclusions	Subjects with mistargeted viral injections or abberant implants (optical, pharmcaological, electrodes) were excluded from analyses. Calcium imaging traces without significant transients were excluded from analyses. Further, corrupted video files prevented blind experimentors from scoring behavior in several marble burying videos. These instanced are stated in the Methods where appropriate.
Replication	Several of our experiments were replicated or cross-verified using a complementary technique. For example: mPFC-dPAG optogenetics/behavior: Cre-DIO behavioral results (i.e., manipulation of mFC-dPAG projectors at the cell body level) were replicated across several cohorts and with terminal manipulations (i.e., manipulation of mPFC-dPAG projectors at the axon terminal level. (Figure 2 and Extended Data Figure 4). in vivo calcium imaging: These data were analyzed using thee distinct methods for ROI detection and fluorescence trace extraction -- 1) a "constrained non-negative matrix factorization (CNMF-E)" algorithm 2) a modified CNMF-E with temporal non-negative constraints removed, and 3) a custom "Non-ROI thresholded background regressed" method. The results are invariant to analysis method and all three results are reported in the manuscript. CNMF-E results are reported in Main Figure 3 and Main Figure 4. Modified CNMF-E and Non-ROI approaches methods are reported in Extended Figure 6 and Extended Data Figure 8. in vivo electrophysiology: This experiment supports our in vivo epifluorescent calcium imaging results from Main Figure 4, using a distinct but complimentary in vivo recording technique. These data support the notion that dopamine enhances signal-to-noise ratio in mPFC-dPAG neurons, specifically for aversive stimuli (Main Figure 4 and Extended Data Figure 9).
Randomization	For most experiments, cagemates were pseudo-randomly assigned to groups during virus injection (i.e., eYFP vs. ChR2). Two stereotaxes were used for viral injection, one equipped with a syringe containing eYFP/contral virus and the other containing ChR2/test virus.
Blinding	During testing, investgators were not blind to condition (i.e., eYFP vs ChR2 or dPAG vs. NAc). However, results were replicated across several cohorts conducted by different investigators. Videos for behavioral scoring (i.e., marble burying experiments) were stripped of identifiers and independently scored by 2 investigators. Other analyses of behavior were automated and analyzed using Noldus Ethovision.

Reporting for specific materials, systems and methods

Materials & experimental systems

n/a	Involved in the study
☒	Unique biological materials
☐	☒ Antibodies
☒	Eukaryotic cell lines
☒	Palaeontology
☐	☒ Animals and other organisms
☒	Human research participants

Methods

n/a	Involved in the study
☒	ChIP-seq
☒	Flow cytometry
☒	MRI-based neuroimaging

Antibodies

Antibodies used	All antibodies used for immunohistochemistry are included in the Extended Methods. Including antibody names, dilutions, and manufacturers.
Validation	All antibodies (TH and c-Fos) used for immunohistochemistry are common and well-validated in the literature.

Animals and other organisms

Policy information about studies involving animals; ARRIVE guidelines recommended for reporting animal research

Laboratory animals	Species, strain, sex, and age are reported for each experiment in the Methods under "Subjects".
Wild animals	n/a
Field-collected samples	n/a